Discovery of 4H-chromeno[2,3-d]pyrimidin-4-one derivatives as senescence inducers and their senescence-associated antiproliferative activities on cancer cells using advanced phenotypic assay

Sangmi Oh, Ji Young Lee, Inhee Choi, Arnaud Ogier, Do Yoon Kwon, Hangyeol Jeong, Sook Jin Son, Youngmi Kim, Haejin Kwon, Seijin Park, et al.

Version of Record: https://www.sciencedirect.com/science/article/pii/S0223523420305225
Manuscript_340e31c516dd8a57ab7de3a4a1c678ac

Discovery of 4*H*-Chromeno[2,3-*d*]pyrimidin-4-one Derivatives as Senescence Inducers and Their Senescence-Associated Antiproliferative Activities on Cancer Cells using Advanced Phenotypic Assay

Sangmi Oh [a, b], Ji Young Lee [c], Inhee Choi [a], Arnaud Ogier [d], Do Yoon Kwon [c], Hangyeol Jeong [c], Sook Jin Son [c], Youngmi Kim [a], Haejin Kwon [e], Seijin Park [e], Hwankyu Kang [e], Kwanghan Kong [e], Sujin Ahn [e], Ulf Nehrbass [c], Myung Jin Kim [c, f, *] and Rita Song [a, *]

[a] *Medicinal Chemistry Group, Institut Pasteur Korea, 16 Daewangpangyo-ro 712 beon-gil, Bundang-gu, Seongnam-si, Gyeonggi-do13488, South Korea*

[b] *Present address: Tuberculosis Research Section, Laboratory of Clinical Immunology and Microbiology, National Institute of Allergy and Infectious Diseases, National Institutes of Health, Bethesda, Maryland 20892, United States*

[c] *Functional Morphometry-I, Institut Pasteur Korea, 16 Daewangpangyo-ro 712 beon-gil, Bundang-gu, Seongnam-si, Gyeonggi-do13488, South Korea*

[d] *Cellular Differentiation and Toxicity Prediction, Institut Pasteur Korea, 16 Daewangpangyo-ro 712 beon-gil, Bundang-gu, Seongnam-si, Gyeonggi-do13488, South Korea*

[e] *Drug Metabolism and Pharmacokinetics, Institut Pasteur Korea, 16 Daewangpangyo-ro 712 beon-gil, Bundang-gu, Seongnam-si, Gyeonggi-do13488, South Korea*

[f] *Present address: New Drug and Bio Research Center, Handok Inc., A-dong, 2nd floor, KoreaBioPark, 700 Daewangpangyo-ro, Bundang-gu, Seongnam-si, Gyeonggi-do 13488, South Korea*

∗ Co-corresponding author.

Tel.: +82-31-698-3832; fax: +82-31-698-3842; e-mail: rsong1228@gmail.com

Tel.: +82-2-527-5036; fax: +82-2-527-5020; e-mail: nanmolra1973@naver.com

Abstract

Current research suggests therapy-induced senescence (TIS) of cancer cells characterized by distinct morphological and biochemical phenotypic changes represent a novel functional target that may enhance the effectiveness of cancer therapy. In order to identify novel small-molecule inducers of cellular senescence and determine the potential to be used for the treatment of melanoma, a new method of high-throughput screening (HTS) and high-contents screening (HCS) based on the detection of morphological changes was designed. This image-based and whole cell-based technology was applied to screen and select a novel class of antiproliferative agents on cancer cells, 4*H*-chromeno[2,3-*d*]pyrimidin-4-one derivatives, which induced senescence-like phenotypic changes in human melanoma A375 cells without serious cytotoxicity against normal cells. To evaluate structure-activity relationship (SAR) study of 4*H*-chromeno[2,3-*d*]pyrimidin-4-one scaffold starting from hit **3**, a focused library containing diversely modified analogues was constructed and which led to the identification of **38**, a novel compound to have remarkable anti-melanoma activity *in vitro* with good metabolic stability.

Keywords

Structure-activity relationship

High-throughput screening

High-contents screening

Senescence

Antiproliferative agents

Melanoma

1. Introduction

Melanoma is the most aggressive form of skin cancer that arises from melanocytes. It is estimated that more than 192,310 new patients per year worldwide and consequently about 7,230 melanoma related deaths occur in 2019 [1, 2]. In the case of early stage of melanomas (stage I and II), the tumor can be surgically resected with high success rate. Whereas five-year survival rates for regional and distant stage melanomas are 64 % and 23 %, respectively [1-4].

Two major drugs for the treatment of patients with metastatic melanoma, including monoclonal antibody to cytotoxic T lymphocyte antigen 4 (CTLA4), ipilimumab, and a selective small molecule inhibitor of V600E mutated BRAF kinase, vemurafenib, have been attributed to an improved understanding of its immune microenvironment and molecular genetics of the disease, respectively [5-7]. However, these two treatments induced serious problems like autoimmune response of ipilimumab [8, 9] and acquired drug resistance to vemurafenib [10, 11]. Even though two new drugs having slightly different mechanism of action, dabrafenib and trametinib, have been recently approved by the FDA, they are only indicated for use in patients with whose tumors express the BRAF V600E gene mutations [12]. Therefore, there is an urgent need to ikdentify novel therapeutic targets and develop novel drug candidates to treat metastatic melanoma.

Over the past several years, acutely stress-responsive forms of cellular senescence have been discovered that seem to play important roles during tumor development. Senescence can effectively function as an *in vivo* tumor suppressor mechanism, limiting proliferation of damaged cells. Mechanistically, senescence is being induced by a variety of pathways involving tumor suppressors such as p53 and retinoblastoma protein (Rb) as well as increased expression of cyclin dependent kinase (CDK) inhibitors including p21 (Cip1/Waf1), p16 (INK4a) and p27 (Kip1) [13]. Current studies have discovered that therapy-induced senescence (TIS), a type of senescence caused by ionizing radiation or genotoxic drugs, could play a critical role in anti-cancer therapy and will provide insights into the development of powerful strategy for therapeutic benefits [14-17]. They have been known to trigger senescence pathways so that senescent states have been observed in breast, melanoma and lung cancers after drug treatment [18-20]. Interestingly, senescence induction followed

by chemotherapy has been correlated with a favorable patient outcome [21]. Furthermore, it was reported that cellular senescence induced by p53 has been associated with tumor clearance and contributed to the outcome of cancer therapy [22]. All these studies underscore the role of senescence in limiting oncogene-initiated tumorigenesis and enhancing the antitumor effects of some cancer drugs [23-27]. Previously, established anti-cancer therapies have been associated with the generation of senescent states *in vivo*, as shown in patients with breast cancer [28] or non-small cell lung cancer [29] after neoadjuvant chemotherapy [17, 30]. Apparently therefore, the strategy of stopping deregulated, malignant cell growth through activation of a senescence program appears feasible even in the advanced stages of melanoma.

In the search for new modulating tools of cellular senescence, senescence-associated β-galactosidase (SA-β-gal) activity of the cells has been generally used in the small-molecule screening as a senescence marker [31, 32]. However, it has a limit for adaptation to the high-throughput assay format due to the use of bright-field microscopy. In this study, we report newly designed image-based assay system for high-throughput screening (HTS) and high-contents screening (HCS), and its application to develop novel small-molecule candidates which induce senescence-like morphological changes. In addition, we report structure-activity relationship (SAR) study of 4*H*-chromeno[2,3-*d*]pyrimidin-4-one derivatives and then *in vitro* biological evaluation of senescence-associated anti-melanoma activities, which chemical scaffold was selected and demonstrated by the novel phenotypic assay for the discovery of senescence inducers. This image-based assay was designed for as a whole cell-based approach that allows for the selection of a new set of compounds based on the unique phenotypes of senescent cells. Focused library was constructed for the improvement of activity and metabolic stability starting from initial hit **3**, which was identified through developed phenotypic screening of commercial library, and then the modified molecule, **38** was developed for *in vivo* study as a consequence.

2. Result and discussion

2.1 Development of phenotypic assay to identify senescence-inducing compounds

To identify novel small molecules to induce cellular senescence and assess their antitumor activities against melanoma cells, novel phenomic assay was developed to measure cellular morphological changes with counting the number of cells in a well. For evaluating senescence-like morphological changes, three different fluorescent dye were used for the cellular staining of nucleus DNA, plasma membrane and lysosomes respectively after fixation of compound-treated cells and then phenotypic changes due to cellular senescence such as enlarged cytoplasm containing a large nuclei and increased cytoplasmic granules were detected. As shown in Fig. 1, this newly developed image-based assay was validated by reference compound, doxorubicin, which is known as a topoisomerase II inhibitor and has been reported to induce the DNA damage-mediated senescence in human cells [33-35]. After the drug treatment for 3 days, stained images of human melanoma A375 cells were acquired and analyzed by customized software which needs segmentation procedure of each stained image before analysis (Fig. 1A). This process has been developed for computational analysis of acquired cellular images to assess diverse information such as number of cells per well, cell size, nucleus size, granule size, the distance of each granules, cytoplasmic texture, and volume of each organelles. As a result, dose-response curves to calculate EC_{50} and IC_{50} were generated based on the analytical data of the number of cells as well as the ratio of senescent cells per well (Fig. 1B). In this study, 'EC' means the effective concentration to induce cellular senescence phenotype, which represents dose-response curve to go uphill. 'IC' means the cell growth inhibitory concentration to reduce cell number, so it is used to express dose-response curve to go downhill. To verify senescence phenotype induced by doxorubicin, A375 cells treated with doxorubicin were also detected with an enhanced activity of SA-β-gal which is a commonly accepted and widely used senescence biomarker (Fig. 1C) [36].

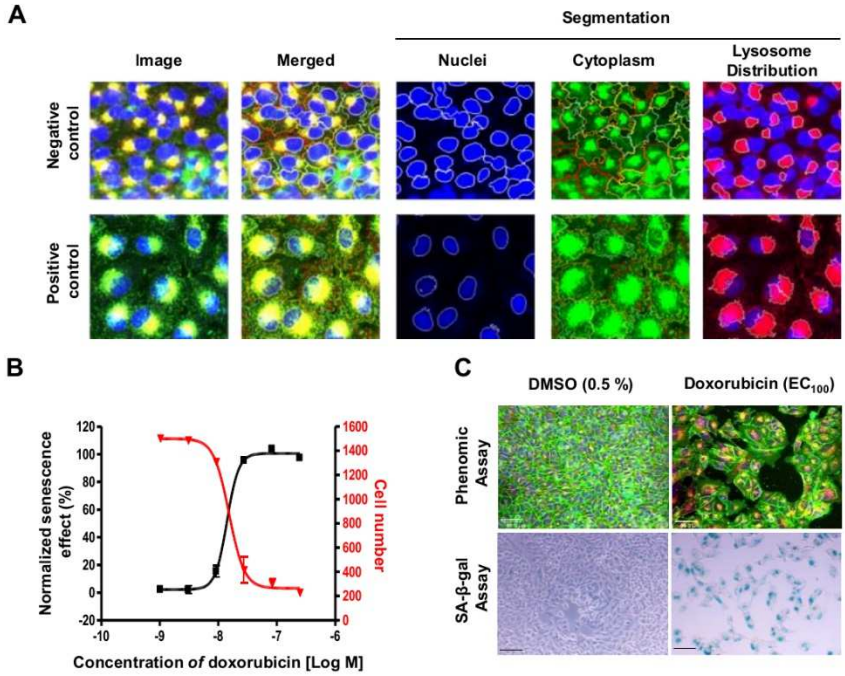

Fig. 1. Assay validation with doxorubicin-treated cells: (A) Segmented images of negative control (0.5 % DMSO) and positive control (37 nM doxorubicin in 0.5 % DMSO) for data analysis. (B) Dose dependent changes of doxorubicin–treated cells. Measurement of cell growth and senescence effect were analyzed by customized algorithm. All experiments were duplicated respectively. (C) Senescence effect of doxorubicin (37 nM in 0.5 % DMSO) in phenomic assay and SA-β-gal assay. Human melanoma A375 cells were treated with or without doxorubicin (37 nM) for 3 days. In phenomic assay, the cells were acquired images after staining with Hoechst 33342, LysoTracker® Red DND-99, and CellMask™ (Upper panel). Under the same condition, cells were performed SA-β-gal (Lower panel) assay. Scale bar is 50 μm.

2.2. Morphological and biochemical changes in human melanoma cells induced by initial hit 3

Compound **3** (Table 1) bearing 4*H*-chromeno[2,3-*d*]pyrimidin-4-one scaffold was one of initial hits selected from the screening of ~110,000 compound library to induce senescence-like morphological changes. The experimental evaluations of **3** were conducted on human melanoma cell line (A375) for particular senescence events in the cell population including SA-β-gal activity, dose response morphological changes, and counting the number of cells with customized image analysis software as well as effects on colony formation and p53 pathway (Fig. 2). As shown in Fig. 2A, compound **3**-treated cells showed senescent phenotypes clearly such as enlarged and flattened morphology with decreased cancer cell proliferation. As compared to the negative control (0.5 % DMSO), morphologically changed A375 cells after the treatment of **3** were also detected with an enhanced activity of SA-β-gal (Fig. 2A). Using customized software, cell images after compound treatment taken from confocal microscopy were analyzed to detect cell number and morphological changes in

dose response. Whereas the number of total cells were decreasing in dose-dependent pattern (IC_{50} = 0.09 μM), the number of morphological changed cells in well were increasing (EC_{50} = 0.11 μM, Fig. 2B).

To check whether these events are irreversible, colony formation assay was performed after 3 days incubation with **3**. When melanoma cells initially treated with small molecule **3** were incubated with fresh media for additional 4 days, they have not been increasing colony number or expanding colony size in the concentration of 2.2 μM as EC_{100} (Fig. 2C).

As noted above, cellular senescence induced by chemotherapy has been known to be closely related to not only the activation of p53 and p21 but also dephosphorylation of Rb. From the result of western blotting experiment shown in Fig. 2D, we confirmed these elevations in the expression of p53 and p21 in compound-treated cells. In addition, another cell cycle arrest marker, Rb was appeared to be dephosphorylated even at the concentration of 0.01 μM. This finding indicates that the activation of p53 signaling pathway after compound treatment underlies the cell cycle arrest and may lead to the cellular senescence.

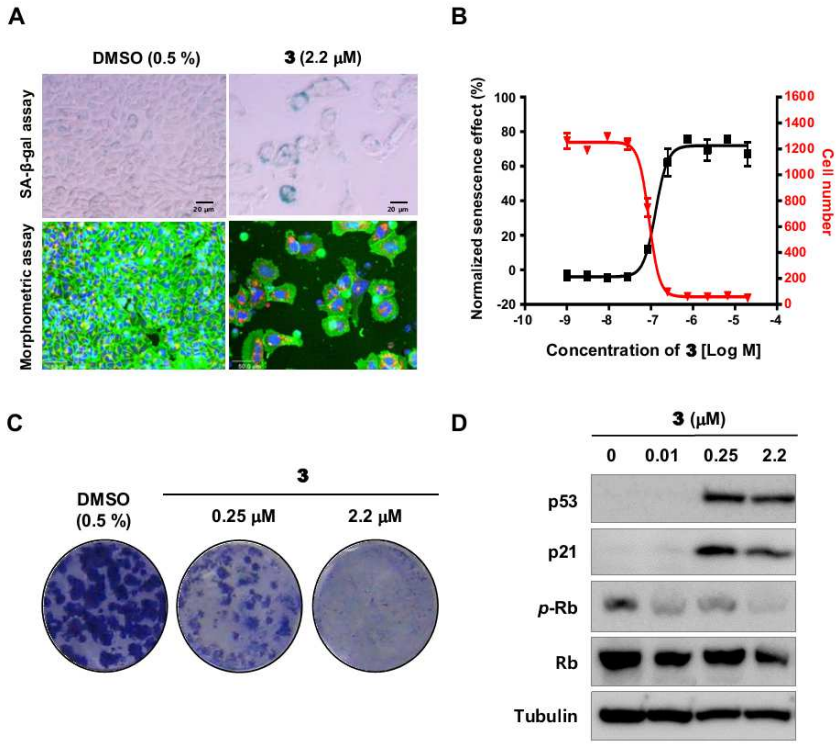

Fig. 2. Activity of **3** in morphological and biochemical changes of human melanoma A375 cells. (A) Results of negative control (0.5 % DMSO) and **3** (EC_{100}, 2.2 μM) after 3 days' incubation in SA-β-gal assay and morphometric assay. (B) Dose-response analysis of **3**. The dose response curves used to determine the EC_{50} (black line) and IC_{50} (red line) values. Black line represents a percentage of senescent cell population in a well. Red line means the number of cells in a well. (C) The effect of **3** in colony formation. Cells were incubated with or without **3** for 72 hrs and then they were cultured in fresh media. Till the formation of colonies, cells were changed media for every 3 days. (D) Biochemical changes of compound-treated cells in western blot. After 3 days treatment of **3**, cells were blotted for p53, p21 and Rb.

2.3. Cellular senescence independent of DNA-damage mechanism

DNA damage response (DDR) is a common feature for monitoring genome integrity [37]. The post-translational modification of DDR factors plays prominent roles in controlling the formation of foci in response to DNA-damaging agents. To define whether the cellular events of **3** are related in DNA-damage mechanism, two different experiments were conducted for the DNA damage analysis: the immunostaining of DNA damage markers, γ-H2AX and 53BP1, and the examination of DNA single-strand break (SSB) formation (Fig. 3A and B).

When cells are exposed to DNA-damaging chemotherapeutic agents like doxorubicin, double-stranded breaks (DSBs) are generated that rapidly result in the phosphorylation of histone H2A variant H2AX. Because phosphorylation of H2AX at Ser^{139} (γ-H2AX) is relevant, and correlates well with each DSB, it is the most sensitive marker that can be used to examine the DNA damage [38]. 53BP1 is also known as a typical marker of DNA damage accomplishing its function in DNA repair [39]. As shown in Fig. 3A, compound **3** did not induce the recruitment of γ-H2AX and 53BP1 in senescent cells, while doxorubicin-treated cells were generated and increased the γ-H2AX and 53BP1 foci in the nuclei, which induces the DNA damage-mediated senescence in human cells [33, 40, 41].

The formation of DNA SSB is a different type of DNA damage response, which is caused by oxidative attack of free radicals generated from cell metabolism or chemotherapeutic agents [37]. In comparison with control cells, however, compound **3** did not promote single-strand breaks in cells (Fig. 3B). In addition, compound effect on cell proliferation was evaluated by measuring the distribution of the cells in the different phases of the cell cycle by flow cytometry. Compound **3** induced statistically significant cell cycle arrest in G2-M phase and Pre-G1 phase as well (Fig. 3C). The ratio of apoptotic cells and senescent cells in sub-G1 fraction was dose-dependently investigated

by the detection of caspase-3 and morphological changes respectively. On the basis of this experiment, we found that small part of cells underwent apoptosis at 72 hrs-treatment (Fig. 3D). We supposed that apoptotic cells at 72 hrs came from fully senescent cells which underwent apoptosis due to continuous stimuli by compound **3**. These results indicated that **3** induced DNA damage-independent cellular senescence through G2-M phase arrest.

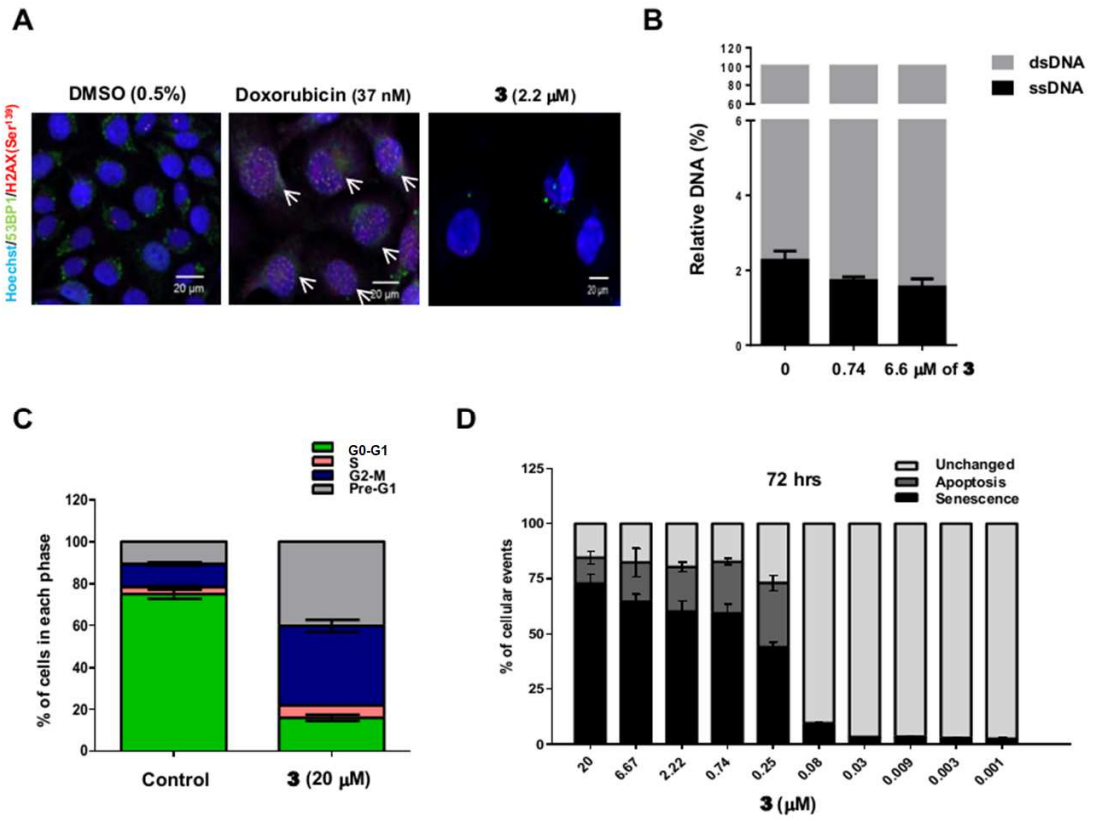

Fig. 3. The effect of **3** in DNA damage mechanism and cell cycle arrest. (A) Recruitment of 53BP1 and γ-H2AX (Ser^{139}) in A375 cells. A375 cells were incubated with or without 37 nM of doxorubicin (Dox) and **3** for 3 days. After fixation, untreated cells, Dox- and **3**-treated cells were incubated with anti-53BP1 and anti-γH2AX. Fluorescent images were acquired by automated confocal microscopy (Opera). White arrows indicated foci in nuclei and scale bar represents 20 μm. (B) Single strand break response of **3**. (C) Cell cycle analysis in A375 cells with 20 μM of **3**. (D) Dose response effect of **3** in apoptosis and cellular senescence. After 3 days treatment, apoptosis and senescence of cell population per well were analyzed by caspase-3 and morphometric changes. All experiments were duplicated respectively.

*2.4. The cell growth inhibition of **3** without any influence in BRAF and NRAS mutations*

The major oncogenic mutations of melanoma are known to be frequently associated with BRAF and/or NRAS kinases [42]. To profile the specificity of **3** against melanoma mutations, compound was tested in six different melanoma cell lines which have different mutations in $BRAF^{V600}$ and $NRAS^{Q61}$

(Fig. 4A). This result showed that compound **3** was more sensitive on some melanoma cell lines, however, its activity was not limited to BRAF and NRAS mutations. Furthermore, compound **3** was also tested in various types of cancer cells associated with different oncogenic mutations, and then examined its specificity of cancer and genetic mutations. As shown in Fig. 3B, similar doses of **3** were needed to inhibit different types of cancer cells with below 1 μM. Although common genetic factors within tested cancer cells have not yet been identified, this finding may lead to the better understanding of mechanism of action when the target protein of **3** might play an important role in a specific signaling pathway related to anti-proliferation on a broad spectrum of cancer cell lines.

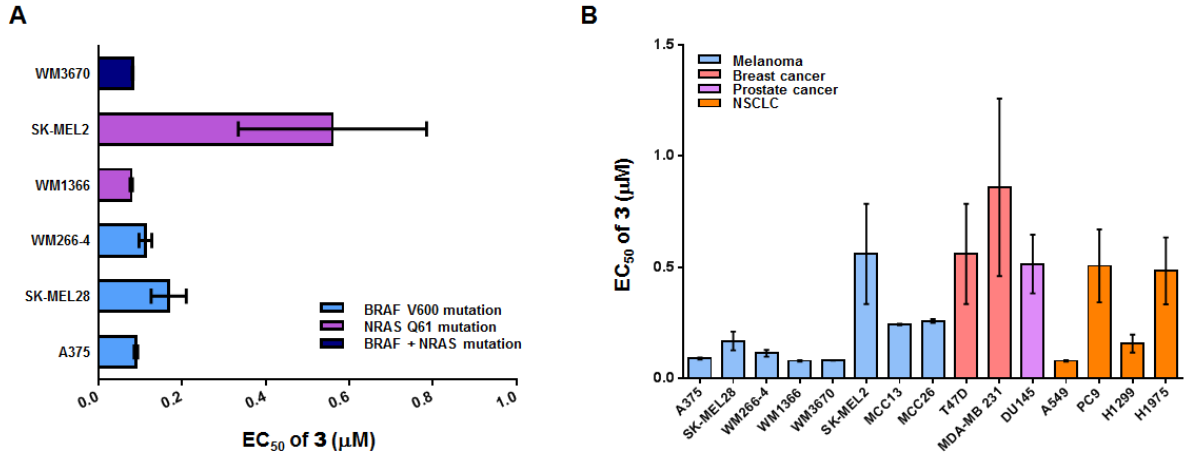

Fig. 4. Cell growth inhibition of **3** in different mutations and cancer types. (A) Growth inhibition of **3** in various melanoma cells containing different mutations. All cells were incubated with **3** for 72 hrs in dose response and then were counted cell numbers. (B) Activity profiling of **3** in various cancer types. All experiments were performed in triplicate.

2.5. Construction of focused library and their structure-activity relationship

To improve senescence-associated anti-melanoma activity and metabolic stability for *in vivo* study, a series of 4*H*-chromeno[2,3-*d*]pyrimidin-4-one analogues were prepared. The synthesis of 4*H*-chromeno[2,3-*d*]pyrimidin-4-one derivatives **A** and their isomers **B** with double bond migration were conducted following the synthetic procedure which was previously reported (Scheme 1) [43, 44]. 2-Iminocoumarin-3-carboxamides **2** were obtained by the reaction of salicylic aldehydes **1** with 2-cyanoactamide in the presence of catalytic amount of piperidine. The interaction of intermediates **2** with aldehydes resulted in a mixture of isomers **A** and **B** in most cases. The ratio of isomers depended

on the structure of the starting aldehyde, the reaction temperature, and the reaction time as previously reported [43, 44]. All final compounds newly synthesized (**4–38**) were characterized by low resolution ESI mass and NMR, the melting points of some compounds were measured as well. Despite several plausible tautomeric structures of final tricyclic ring, a singlet -CH_2- in pyran ring of **B** observed in the range of near 4 ppm was clearly differentiated from -CH- of **A** type tautomers observed in the downfield based on the proton NMR spectra. *In vitro* activities inducing senescence-like phenotype (EC_{50}) and anti-proliferative activities (IC_{50}) of synthetic compounds were summarized in Table 1.

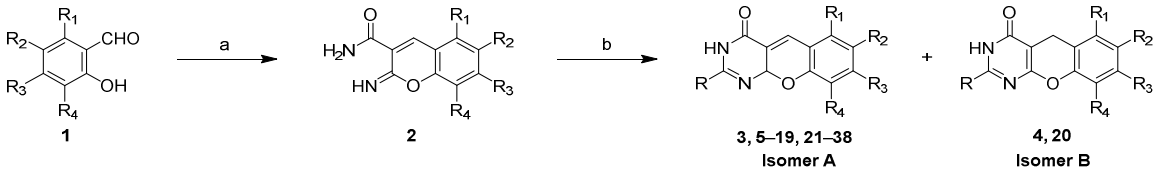

Scheme 1. Synthesis for analogues **3–38**. Reagents and conditions: (a) 2-cyanoacetamide, piperidine, EtOH; (b) RCHO, piperidine, *n*-pentanol.

Table 1. Activity inducing senescence-like phenotype (EC_{50}) and anti-proliferative activity (IC_{50}) of synthetic 4*H*-chromeno[2,3-*d*]pyrimidin-4-one derivatives

No.	Chemical Structure						Activity (μM)	
	Scaffold	R	R^1	R^2	R^3	R^4	EC_{50}[a]	IC_{50}[b]
3	A	4-hydroxyphenyl	–$(CH)_4$–		H	H	0.11	0.09
4	B	4-hydroxyphenyl	–$(CH)_4$–		H	H	1.19	0.64
5	A	4-hydroxyphenyl	H	H	H	H	> 20	6.60
6	A	4-hydroxyphenyl	H	fluoro	H	H	15.0	0.37
7	A	4-hydroxyphenyl	H	methyl	H	H	0.57	0.19
8	A	4-hydroxyphenyl	H	ethyl	H	H	0.10	0.02
9	A	4-hydroxyphenyl	H	*iso*propyl	H	H	0.09	0.10
10	A	4-hydroxyphenyl	H	*tert*butyl	H	H	0.20	0.20
11	A	4-hydroxyphenyl	H	phenyl	H	H	0.14	0.22
12	A	4-hydroxyphenyl	H	3-furyl	H	H	0.27	0.33
13	A	4-hydroxyphenyl	H	methoxy	H	H	0.19	0.31
14	A	4-hydroxyphenyl	H	phenoxy	H	H	0.32	0.28
15	A	4-hydroxyphenyl	H	dimethylamino	H	H	0.59	0.47
16	A	4-hydroxyphenyl	H	morpholino	H	H	11.0	6.00
17	A	4-hydroxyphenyl	H	H	diethylamino	H	> 20	18.0
18	A	4-hydroxyphenyl	H	*tert*butyl	H	*tert*butyl	> 20	> 20
19	A	phenyl	H	*iso*propyl	H	H	0.01	0.01
20	B	phenyl	H	*iso*propyl	H	H	0.28	0.26
21	A	benzyl	H	*iso*propyl	H	H	> 20	> 20

22	A	cyclohexyl	H	*iso*propyl	H	H	> 20	> 20
23	A	cyclopropyl	H	*iso*propyl	H	H	> 20	> 20
24	A	*iso*propyl	H	*iso*propyl	H	H	> 20	> 20
25	A	2-thiophenyl	H	*iso*propyl	H	H	0.04	0.08
26	A	3-hydroxyphenyl	H	*iso*propyl	H	H	0.11	0.06
27	A	2-hydroxyphenyl	H	*iso*propyl	H	H	3.00	6.00
28	A	4-fluorophenyl	H	*iso*propyl	H	H	7.00	0.52
29	A	3-fluorophenyl	H	*iso*propyl	H	H	0.25	0.20
30	A	3-methoxyphenyl	H	*iso*propyl	H	H	0.03	0.01
31	A	4-toluyl	H	*iso*propyl	H	H	0.09	0.01
32	A	4-dimethylaminophenyl	H	*iso*propyl	H	H	> 20	3.00
33	A	3-fluoro-4-hydroxyphenyl	H	*iso*propyl	H	H	0.10	0.05
34	A	2-fluoro-4-hydroxyphenyl	H	*iso*propyl	H	H	0.94	0.28
35	A	4-hydroxy-3-methoxyphenyl	H	*iso*propyl	H	H	0.08	0.04
36	A	5-benzodioxol	H	*iso*propyl	H	H	0.09	0.08
37	A	2,3-dimethoxyphenyl	H	*iso*propyl	H	H	20.0	4.00
38	A	2,3-dimethylphenyl	H	*iso*propyl	H	H	0.003	0.004
Doxorubicin							0.009	0.011

[a] EC_{50} means the effective concentration of a drug that induces senescence in a half population. [b] IC_{50} represents the dose of a compound where the cell number is reduced by 50 %.

To investigate structure-activity relationships, 36 analogues of initial hit **3** were synthesized and evaluated their activities inducing senescence-like phenotype (EC_{50}) and anti-proliferative activities (IC_{50}). In this experiment, a known chemotherapeutic agent, doxorubicin, was used as a positive control, which induces cellular senescence via inhibition of topoisomerase II and DNA damage under low concentration [33, 41]. A comparison of scaffolds **A** and **B** had been a priority for the construction of focused library. Compounds **4** (1.19 μM) and **20** (0.28 μM) bearing scaffold **B**, which are the counterparts of initial hit **3** (0.11 μM) and **19** (0.01 μM) bearing scaffold **A**, respectively, showed significant decrease of activities to induce senescence-like phenotype more than 10-fold. This finding indicated that conformational change of main structure, 4*H*-chromeno[2,3-*d*]pyrimidin-4-one, caused by double bond migration might influence on the binding event of putative target biomolecules. In terms of substituent effects on tricyclic benzene ring (R^1–R^4), the presence of electron donating and hydrophobic alkyl or aryl substituent at R^2 such as ethyl (**8**), isopropyl (**9**), and phenyl (**11**) was necessary to retain activities so that they showed promising EC_{50} values (0.10, 0.09, and 0.14 μM, respectively) similar to that of **3**, which fused with benzene to make tetracyclic ring from R^1 to R^2. Whereas other derivatives with electronegative fluorine (**6**) or hydrophilic morpholine (**16**) at the

same position as well as the analogue without substituent (**5**) were significantly losing their activities or even inactive. Alkyl substituents at R^4 was not good for the activity because **8** having two *tert*butyl groups at R^2 and R^4 was found to be inactive while **10** having one *tert*butyl group at R^2 showed promising activity with 0.26 μM. In addition, hydrophilic substituent at R^3 like diethylamino group (**17**) was not effective for the improvement of activity while **15** having dimethylamino group at R^2 showed moderate activity with 0.59 μM.

To assess the importance of R, a series of compounds **19–38** were synthesized and evaluated their activities to stimulate senescence-like morphological change. All analogues described here embedded with isopropyl group at R^2 instead of fused benzene because **9** showed improved activity in comparison with initial hit **3** (Tables 1 and 2). As shown in Table 1, phenyl group in the position of R was essential for maintaining activity due to the fact that synthetic analogues to have benzyl (**21**) or the saturated hydrocarbons such as cyclohexyl (**22**), cyclopropyl (**23**), and isopropyl (**24**) were found to be inactive. In the search for proper substituents on the phenyl ring in the R, various substituents with different electronic effects, different hydrogen bonding properties, or different position were applied in the phenyl ring, and then finally **38** bearing two methyl groups in *ortho*- and *meta*-positions was selected as the most potent compound in the focused library with the activity of 3 nM, which was an activity inducing senescence-like phenotype comparable to that of reference drug, doxorubicin (9 nM). As shown in Table 1, anti-proliferative activities of all synthetic analogues designated by IC_{50} were correlated well with the corresponding EC_{50} which were determined by image-based senescence-inducing activities. In addition to the promising improvement of anti-proliferative activity related to senescence, dimethyl substituted-phenyl embedded-molecule **38** was metabolically stable, demonstrating significant improvement in the intrinsic clearance against both human and mouse liver microsomes (Table 2).

Table 2. Metabolic stability of synthetic 4*H*-chromeno[2,3-*d*]pyrimidin-4-one derivatives

Compound	Metabolic Stability ($T_{1/2}$[a], min)	
	Phase I	Phase II[b]

	Human	Mouse	Human	Mouse
3	43.6	9.30	N/T[c]	N/T
8	32.5	7.97	N/T	N/T
9	>60	13.0	N/T	N/T
19	39.7	11.8	N/T	N/T
20	>60	30.1	17.8	17.4
25	21.6	6.56	N/T	N/T
26	37.6	6.65	N/T	N/T
29	14.7	8.47	N/T	N/T
30	32.9	14.7	N/T	N/T
31	32.0	6.44	N/T	N/T
33	57.1	13.2	N/T	N/T
35	>60	20.2	>60	2.88
36	32.5	18.6	N/T	N/T
38	51.6	54.9	>60	>60

[a] $T_{1/2}$ means the time which the concentration of a drug is reduced by half for 1 hr incubation. [b] Glucuronidation only. [c] N/T not tested.

Based on the data of metabolic stability, **38** was selected for mouse pharmacokinetics (PK) study. As indicated in Table 3, **38** demonstrated modest oral bioavailability with acceptable half-lives in blood circulation, suggesting strong possibility that a series of 4*H*-chromeno[2,3-*d*]pyrimidin-4-one analogues could be developed as oral drugs. Even though the intraperitoneal (IP) administration gave 2-fold higher AUC and prolonged $t_{1/2}$ than oral (PO) administration, PK profile of **38** did not exhibit *in vivo* efficacy which could be explained by *in vitro* EC_{50} correction with plasma protein binding. Therefore, optimization of the series of compounds is required to improve drug-like properties, maintaining their *in vitro* activities. Currently further optimization of compounds is underway to improve oral PK parameters that are expected to show *in vivo* efficacy in xenograft model.

Table 3. Pharmacokinetic parameters for **38** in mice

Admin	Dose (mg/kg)	C_0[a]/C_{max}[b] (ng/mL)	$t_{1/2}$[c] (h)	AUC_{last}[d] (ng×h/mL)	CL[e] (mL/min/kg)	V_{dss}[f] (mL/kg)	MRT[g] (h)	F[h] (%)
IV	2	446	1.26	265	116	8714	0.870	N/A[i]
PO	10	142	3.57	479	N/A	N/A	3.78	36.1
IP	10	380	9.32	1397	N/A	N/A	4.95	105

[a] C_0 means concentration at time 0 hr for IV. [b] C_{max} means maximum concentration for PO and IP. [c] $t_{1/2}$ indicates half-life. [d] AUC_{last} means area under the curve from 0 to 24 hr. [e] CL means systemic clearance. [f] V_{dss} means volume of distribution at steady-state. [g] MRT means mean residence time. [h] F means oral bioavailability. [i] N/A not available.

2.6. Pharmacophore modeling

To investigate SAR of 4*H*-chromeno[2,3-*d*]pyrimidin-4-one derivatives, total of eight common pharmacophore hypotheses (CPH) featuring six pharmacophore sites were developed. Based on survival score, AAHPRR.2 was selected as the best CPH having the highest score (8.105) than others. It consists of two H-bond acceptors (A), one hydrophobic (H), two aromatic rings (R), and one positive ionizable (P) features. Active ligands were well aligned with all six pharmacophoric features such as the most active compound, **38** (Fig. 5A). The conformation difference of the main structure, 4*H*-chromeno[2,3-*d*]pyrimidin-4-one, was clearly distinguished between scaffolds **A** and **B**. The conformation of **3** with the scaffold **A** was puckered up above the plane at the saturated pyrimidine ring. However, the centroid of P8 feature was not aligned with the nitrogen atom in the pyrimidine ring in the scaffold **B** of **4** (10-fold less active) due to a flat conformation caused by double bond migration (Fig. 5B). The contribution of phenyl group or aromaticity in the position of R in biological activities were validated with the pharmacophore mapping results. Analogues **21** with benzyl and **24** with isopropyl substituents in the position of R were mapped with only five features of CPH. These substituents of those inactive compounds failed to map with the aromatic ring feature, R10 (Fig. 5C). In case of R^2 position, the presence of electron donating and hydrophobic alkyl or aryl substituents at R^2 were very important for the good biological activity of the compounds. When there is no substituent in this position like compound **5**, the activity was significantly lost suggested by H7 feature not matching with **5** (Fig. 5D). Having a substituent in different position like a diethylamino group in R^3 of **17** was also not effective for the anti-proliferative activity. The orientation of most of the features mapped with **17** (Fig. 5D) were moved away from the centroid.

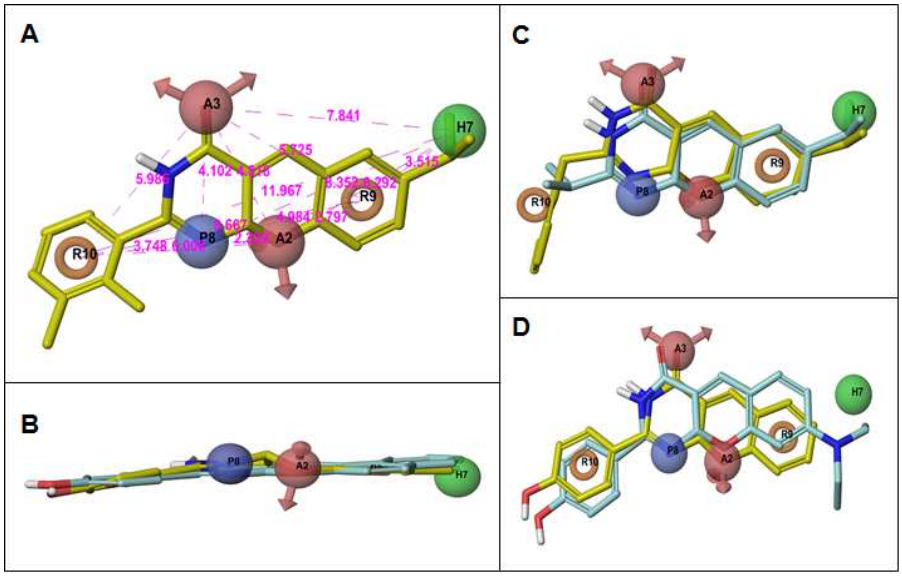

Fig. 5. (A) The best CPH, AAHPRR.2, is superimposed with the best compound, **38** (yellow). Two aromatic ring features (R9 and R10), two H-bond acceptor features with lone pairs of electron (A2 and A3), one positive ionizable (P8) feature, and one hydrophobic feature (H7) are shown in orange rings, pink spheres, blue sphere, and green sphere, respectively. The distances between pharmacophoric features are shown in magenta dotted lines with values. (B) Conformational difference in scaffolds A and B are shown between compounds **3** (yellow) and **4** (light blue). (C) The substituents in R position of inactive compounds **21** (yellow) and **24** (light blue) did not map with R10 feature. (D) Inactive compounds, **5** (yellow) with no R^2 substituent and **17** (light blue) with a hydrophilic R^3 substituent, did not map with H7 feature.

3. Conclusion

Due to the fact that cellular senescence is characterized by a sustained growth arrest and is commonly observed in premalignant lesions, it has been supporting the notion that senescence acts as a potent tumor suppressor mechanism restricting cell proliferation [21]. A series of 4*H*-chromeno[2,3-*d*]pyrimidin-4-one derivatives were identified as a novel class of anti-proliferative agents associated with senescence. For the selection and evaluation of small-molecule hits, advanced image-based assay was designed for high-throughput screening (HTS) and high-contents screening (HCS) as a whole cell-based approach that could recognize the unique phenotypes of senescent cells. The hit compound, **3** was initially confirmed as an inducer of senescence-associated morphological changes in high-throughput phenotypic screening, which was accompanied by anti-proliferative activity against melanoma cells without DNA damage. The dose dependent senescence effect of **3** in melanoma cells corresponded to a cell cycle arrest in G2-M phase and did not relate to BRAF and NRAS mutations. In addition, cancer profiling data suggests that the sensitivity of cancer cells against **3** was independent on cancer type. Together, our results provide the possibility of senescence as an

alternative anti-cancer therapy even though the mechanism should be investigated more. After constructing a series of analogues derived from **3**, analysis of the structure-activity relationship revealed that 2-phenyl and 5-alkyl substituents, especially ^{iso}propyl, on 4*H*-chromeno[2,3-*d*]pyrimidin-4-one tricyclic ring played a critical role to display anti-proliferative activity. In addition, hydrophobic dimethyl substituents in 2-phenyl ring enhanced metabolic stability so that **38** was finally selected for *in vivo* PK study. This advanced molecule was a potential candidate to be suitable for oral administration with modest oral bioavailability and appropriate intrinsic clearance. Further optimization of compounds is on-going to improve oral PK parameters and *in vivo* efficacy study in xenograft model. According to the developed pharmacophore model, the best CPH generated, AAHHRR.2, was found to be predictive in differentiating active and inactive 4*H*-chromeno[2,3-*d*]pyrimidin-4-one analogues based on senescence-associated antitumor activity. It predicted the aromatic ring (R10) as well as the hydrophobic (H7) features as important determinants in biological activity. In addition, one positive ionizable (P8) and two H-bond acceptor features (A2 and A3) were critical in sustaining the conformational difference between saturated and unsaturated main scaffold, 4*H*-chromeno[2,3-*d*]pyrimidin-4-one.

Even though the molecular mechanism of senescence in particular of melanoma cells remains to be examined in detail, it is no doubt that cellular senescence is an attractive therapeutic strategy to prevent melanoma cell proliferation. In this regard, 4*H*-chromeno[2,3-*d*]pyrimidin-4-one derivatives will be a good starting point to develop novel small-molecule probes exploring the potential targets for pro-senescence drugs. A follow-up studies including optimization of *in vivo* efficacy and elucidation of mechanism of action are currently underway.

4. Experimental section

4.1. General chemistry information

^{1}H and ^{13}C NMR spectra were recorded on a Varian High Resolution FT-NMR Spectrometer-400, and chemical shifts were measured in ppm relative to internal tetramethylsilane (TMS) standard or specific solvent signal. Routine mass analyses were performed on Waters LC/MS ZQ2000 system equipped with a reverse phase column (XBridge™ C18 × 3.5 μm, 50 × 2.1 mm) and photodiode array detector using electron spray ionization (ESI). The gradient mobile phase consisting of acetonitrile / water with 0.1% formic acid and UV detection at 254 and 210 nm were used to confirm all final products to be ≥95%. Melting point analyses were performed on BUCHI Melting point M-565. Most reagents used in the synthetic procedure were purchased from Sigma-Aldrich, Alfa Aesar, and TCI. The progress of reaction was monitored using thin-layer chromatography (TLC) (silica gel 60 F_{254} 0.25 mm), and the products were visualized by UV light (254 and 365 nm) or by ninhydrin staining followed by heating. Silica gel 60 (0.040–0.063 mm) used in flash column chromatography was purchased from Merck. Other solvents and organic reagents were purchased from commercial venders and used without further purification unless otherwise mentioned.

*4.1.1. Synthetic procedure for 4H-chromeno[2,3-d]pyrimidin-4-one derivatives A and their isomers B (**3–38**)*

All compounds **3–38** were obtained using the previously reported procedure with small modification. Briefly, to a stirred solution of salicylic aldehydes **1** (1.0 eq.) and 2-cyanoacetamide (1.1 eq.) in ethanol, piperidine was added (0.05 eq.). The reaction mixture was stirred for about 5 hrs at room temperature. After the reaction was completed, the solid was filtered and washed with ethanol and dried *in vacuo* to give desired 2-iminocoumarin-3-carboxamide derivatives (**2**) with 60–80 % yields. Compounds **2** was added to a stirring mixture of corresponding aldehyde (RCHO, 1.5 eq.) and piperidine (2.0 eq.) in *n*-pentanol. The reaction mixture in the sealed bottle was heated (120–140 ˚C) for about 10 min. After the reaction was completed, the reaction mixture cooled down to room temperature. The solid was filtered and washed with ethanol and dried *in vacuo* to give desired

product. In case solid was not generated, the reaction mixture was evaporated and then purified by flash column chromatography (methanol / CH_2Cl_2) to give desired product.

*9-(4-Hydroxyphenyl)-7aH-benzo[5,6]chromeno[2,3-d]pyrimidin-11(10H)-one (**3**).* Yellow solid; ^{1}H NMR (400 MHz, DMSO-d_6) δ 9.45 (s, 1H, OH), 8.94 (s, 1H, NH), 8.63 (s, 1H, C-CH-C), 8.46 (d, *J* = 8.4 Hz, 1H, Ar-H), 8.13 (d, *J* = 8.8 Hz, 1H, Ar-H), 8.00 (d, *J* = 8.0 Hz, 1H, Ar-H), 7.70 (t, *J* = 7.6 Hz, 1H, Ar-H), 7.57 (t, *J* = 7.4 Hz, 1H, Ar-H), 7.42 (d, *J* = 8.8 Hz, 1H, Ar-H), 7.18 (d, *J* = 8.4 Hz, 2H, Ar-H in R), 6.76 (d, *J* = 8.4 Hz, 2H, Ar-H in R), 6.20 (s, 1H, N-CH-O); LC/MS (ESI) m/z 343 $[M+H]^+$.

*9-(4-Hydroxyphenyl)-10H-benzo[5,6]chromeno[2,3-d]pyrimidin-11(12H)-one (**4**).* Yellow solid; mp = 267.3 ˚C; ^{1}H NMR (400 MHz, DMSO-d_6) δ 8.06 (d, *J* = 8.8 Hz, 2H, Ar-H in R), 7.98–7.90 (m, 3H, Ar-H), 7.66 (t, *J* = 7.6 Hz, 1H, Ar-H), 7.54 (t, *J* = 7.6 Hz, 1H, Ar-H), 7.38 (d, *J* = 8.8 Hz, 1H, Ar-H), 6.89 (d, *J* = 8.8 Hz, 2H, Ar-H in R), 4.02 (s, 2H, -CCH_2C-); LC/MS (ESI) m/z 343 $[M+H]^+$.

*2-(4-Hydroxyphenyl)-3H-chromeno[2,3-d]pyrimidin-4(10aH)-one (**5**).* Pale yellow solid; ^{1}H NMR (400 MHz, DMSO-d_6) δ 9.45 (s, 1H, OH), 8.91 (s, 1H, NH), 8.00 (s, 1H, Ar-H), 7.67 (dd, *J* = 7.6 and 1.6 Hz, 1H, Ar-H), 7.53–7.49 (m, 1H, Ar-H), 7.23–7.18 (m, 2H, Ar-H), 7.14 (d, *J* = 8.4 Hz, 2H, Ar-H in R), 6.74 (d, *J* = 8.4 Hz, 2H, Ar-H in R), 6.13 (s, 1H, N-CH-O); LC/MS (ESI) m/z 293 $[M+H]^+$.

*7-Fluoro-2-(4-hydroxyphenyl)-3H-chromeno[2,3-d]pyrimidin-4(10aH)-one (**6**).* Yellow solid; ^{1}H NMR (400 MHz, DMSO-d_6) δ 9.47 (bs, 1H, OH), 8.99 (s, 1H, NH), 7.99 (s, 1H, Ar-H), 7.58 (dd, *J* = 8.6 and 3.0 Hz, 1H, Ar-H), 7.37 (td, *J* = 8.6 and 3.2 Hz, 1H, Ar-H), 7.25–7.22 (m, 1H, Ar-H), 7.14 (d, *J* = 8.4 Hz, 2H, Ar-H in R), 6.75 (d, *J* = 8.4 Hz, 2H, Ar-H in R), 6.13 (s, 1H, N-CH-O); LC/MS (ESI) m/z 311 $[M+H]^+$.

*2-(4-Hydroxyphenyl)-7-methyl-3,10a-dihydro-4H-chromeno[2,3-d]pyrimidin-4-one (**7**).* Yellow solid; mp = 270.2 ˚C; ^{1}H NMR (400 MHz, DMSO-d_6) δ 9.45 (s, 1H, OH), 8.89 (s, 1H, NH), 7.94 (s, 1H, Ar-H), 7.46 (d, *J* = 1.6 Hz, 1H, Ar-H), 7.32 (dd, *J* = 8.4 and 1.6 Hz, 1H, Ar-H), 7.13 (d, *J* = 8.8 Hz, 2H, Ar-H in R), 7.09 (d, *J* = 8.4 Hz, 1H, Ar-H), 6.74 (d, *J* = 8.8 Hz, 2H, Ar-H in R), 6.11 (s, 1H, N-CH-O), 2.30 (s, 3H, CH3); LC/MS (ESI) m/z 307 $[M+H]^+$.

*7-Ethyl-2-(4-hydroxyphenyl)-3,10a-dihydro-4H-chromeno[2,3-d]pyrimidin-4-one (**8**).* Pale yellow solid; ^{1}H NMR (400 MHz, DMSO-d_6) δ 9.45 (s, 1H, OH), 8.90 (s, 1H, NH), 7.95 (s, 1H, Ar-H), 7.51

(d, *J* = 2.0 Hz, 1H, Ar-H), 7.36 (dd, *J* = 8.4 and 2.0 Hz, 1H, Ar-H), 7.14–7.10 (m, 3H, Ar-H), 6.74 (d, *J* = 8.8 Hz, 2H, Ar-H in R), 6.11 (s, 1H, N-CH-O), 2.60 (q, *J* = 7.6 Hz, 2H, -CH_2CH_3), 1.19 (t, *J* = 7.6 Hz, 3H, -CH_2CH_3); LC/MS (ESI) m/z 321 $[M+H]^+$.

2-(4-Hydroxyphenyl)-7-isopropyl-3,10a-dihydro-4H-chromeno[2,3-d]pyrimidin-4-one ***(9)****.* Pale yellow solid; ^{1}H NMR (400 MHz, DMSO-d_6) δ 9.45 (s, 1H, OH), 8.89 (s, 1H, NH), 7.97 (s, 1H, Ar-H), 7.55 (d, *J* = 1.6 Hz, 1H, Ar-H), 7.40 (d, *J* = 8.6 and 2.2 Hz, 1H, Ar-H), 7.12 (t, *J* = 8.0 Hz, 3H, Ar-H), 6.74 (d, *J* = 8.6 Hz, 2H, Ar-H in R), 6.11 (s, 1H, N-CH-O), 2.93–2.85 (m, 1H, -$CH(CH_3)_2$), 1.21 (d, *J* = 6.8 Hz, 6H, -$CH(CH_3)_2$); LC/MS (ESI) m/z 335 $[M+H]^+$.

7-(tert-Butyl)-2-(4-hydroxyphenyl)-3,10a-dihydro-4H-chromeno[2,3-d]pyrimidin-4-one ***(10)****.* Pale yellow solid; ^{1}H NMR (400 MHz, DMSO-d_6) δ 9.44 (s, 1H, OH), 8.88 (s, 1H, NH), 8.01 (s, 1H, Ar-H), 7.71 (d, *J* = 2.4 Hz, 1H, Ar-H), 7.40 (d, *J* = 8.8 and 2.4 Hz, 1H, Ar-H), 7.14–7.11 (m, 3H, Ar-H), 6.74 (d, *J* = 8.4 Hz, 2H, Ar-H in R), 6.11 (s, 1H, N-CH-O), 1.29 (s, 9H, ^{t}Bu); LC/MS (ESI) m/z 349 $[M+H]^+$.

2-(4-Hydroxyphenyl)-7-phenyl-3H-chromeno[2,3-d]pyrimidin-4(10aH)-one ***(11)****.* Yellow solid; ^{1}H NMR (400 MHz, DMSO-d_6) δ 9.45 (s, 1H, OH), 8.95 (s, 1H, NH), 8.06 (s, 1H, Ar-H), 8.02 (d, *J* = 2.0 Hz, 1H, Ar-H), 7.82 (dd, *J* = 8.4 and 2.0 Hz, 1H, Ar-H), 7.69 (d, *J* = 8.4 Hz, 2H, Ar-H), 7.51–7.46 (m, 3H, Ar-H), 7.41–7.37 (m, 1H, Ar-H), 7.29 (d, *J* = 8.4 Hz, 1H, Ar-H), 7.16 (d, *J* = 8.4 Hz, 2H, Ar-H in R), 6.75 (d, *J* = 8.4 Hz, 2H, Ar-H in R), 6.15 (s, 1H, N-CH-O); LC/MS (ESI) m/z 369 $[M+H]^+$.

7-(Furan-3-yl)-2-(4-hydroxyphenyl)-3H-chromeno[2,3-d]pyrimidin-4(10aH)-one ***(12)****.* Yellow solid; mp = 241.8 ˚C; ^{1}H NMR (400 MHz, DMSO-d_6) δ 9.45 (s, 1H, OH), 8.95 (s, 1H, NH), 8.18 (s, 1H, Ar-H), 7.96 (s, 1H, Ar-H), 7.93 (d, *J* = 2.0 Hz, 1H, Ar-H), 7.77–7.75 (m, 2H, Ar-H), 7.22 (d, *J* = 8.4 Hz, 1H, Ar-H), 7.15 (d, *J* = 8.4 Hz, 2H, Ar-H in R), 6.96 (s, 1H, Ar-H), 6.75 (d, *J* = 8.4 Hz, 2H, Ar-H in R), 6.14 (s, 1H, N-CH-O); ^{13}C NMR (100 MHz, DMSO-d_6) δ 159.1, 157.6, 154.3, 152.8, 145.0, 139.8, 133.1, 133.0, 130.5, 128.4, 127.9, 126.7, 125.0, 119.8, 116.5, 115.6, 115.4, 109.1, 71.2; LC/MS (ESI) m/z 359 $[M+H]^+$.

2-(4-Hydroxyphenyl)-7-methoxy-3H-chromeno[2,3-d]pyrimidin-4(10aH)-one ***(13)****.* Yellow solid; mp = 267.7 ˚C; ^{1}H NMR (400 MHz, DMSO-d_6) δ 9.44 (s, 1H, OH), 8.91 (s, 1H, NH), 7.97 (s, 1H, Ar-

H), 7.28 (d, *J* = 2.8 Hz, 1H, Ar-H), 7.15–7.08 (m, 4H, Ar-H), 6.74 (d, *J* = 8.8 Hz, 2H, Ar-H in R), 6.11 (s, 1H, N-CH-O), 3.77 (s, 3H, -OCH_3); ^{13}C NMR (100 MHz, DMSO-d_6) δ 159.2, 157.6, 155.7, 154.5, 148.1, 133.31, 133.27, 127.9, 119.9, 119.8, 117.0, 115.6, 115.3, 113.3, 71.1; LC/MS (ESI) m/z 323 $[M+H]^+$.

2-(4-Hydroxyphenyl)-7-phenoxy-3,10a-dihydro-4H-chromeno[2,3-d]pyrimidin-4-one ***(14)****.* Pale yellow solid; ^{1}H NMR (400 MHz, DMSO-d_6) δ 9.46 (s, 1H, OH), 8.95 (s, 1H, NH), 8.00 (s, 1H, Ar-H), 7.44 (d, *J* = 2.4 Hz, 1H, Ar-H), 7.39 (t, *J* = 8.0 Hz, 2H, Ar-H), 7.24–7.12 (m, 5H, Ar-H), 7.01 (d, *J* = 8.8 Hz, 2H, Ar-H in R), 6.75 (d, *J* = 8.4 Hz, 2H, Ar-H in R), 6.13 (s, 1H, N-CH-O); ^{13}C NMR (100 MHz, DMSO-d_6) δ 159.0, 157.6, 157.5, 154.3, 152.3, 150.1, 133.1, 132.9, 130.6, 127.9, 124.3, 123.8, 120.7, 119.9, 118.3, 117.6, 115.60, 115.58, 71.2; LC/MS (ESI) m/z 385 $[M+H]^+$.

7-(Dimethylamino)-2-(4-hydroxyphenyl)-3,10a-dihydro-4H-chromeno[2,3-d]pyrimidin-4-one ***(15)****.* Yellow solid; mp = 262.4 ˚C; ^{1}H NMR (400 MHz, DMSO-d_6) δ 9.44 (s, 1H, OH), 8.86 (s, 1H, NH), 7.95 (s, 1H, Ar-H), 7.12 (d, *J* = 8.4 Hz, 2H, Ar-H in R), 7.05 (d, *J* = 9.2 Hz, 1H, Ar-H), 7.00 (d, *J* = 2.8 Hz, 1H, Ar-H), 6.93 (dd, *J* = 8.8 and 2.8 Hz, 1H, Ar-H), 6.74 (d, *J* = 8.4 Hz, 2H, Ar-H in R), 6.09 (s, 1H, N-CH-O), 2.89 (s, 6H, -$N(CH_3)_2$); ^{13}C NMR (100 MHz, DMSO-d_6) δ 159.4, 157.5, 154.7, 147.7, 145.7, 134.1, 133.5, 127.8, 119.6, 118.0, 116.3, 115.5, 115.0, 112.3, 71.1, 41.0; LC/MS (ESI) m/z 336 $[M+H]^+$.

2-(4-Hydroxyphenyl)-7-morpholino-3,10a-dihydro-4H-chromeno[2,3-d]pyrimidin-4-one ***(16)****.* Yellow solid; mp = 274.2 ˚C; ^{1}H NMR (400 MHz, DMSO-d_6) δ 9.44 (s, 1H, OH), 8.88 (s, 1H, NH), 7.93 (s, 1H, Ar-H), 7.23 (d, *J* = 2.8 Hz, 1H, Ar-H), 7.17–7.08 (m, 4H, Ar-H), 6.74 (d, *J* = 8.4 Hz, 2H, Ar-H in R), 6.10 (s, 1H, N-CH-O), 3.76–3.74 (m, 4H, -NCH_2CH_2O-), 3.10–3.08 (m, 4H, -NCH_2CH_2O-); LC/MS (ESI) m/z 378 $[M+H]^+$.

7-(Diethylamino)-2-(4-hydroxyphenyl)-3H-chromeno[2,3-d]pyrimidin-4(10aH)-one ***(17)****.* Yellow solid; mp = 212.4 ˚C; ^{1}H NMR (400 MHz, DMSO-d_6) δ 9.41 (s, 1H, OH), 8.49 (s, 1H, NH), 7.81 (s, 1H, Ar-H), 7.38 (d, *J* = 8.8 Hz, 1H, Ar-H), 7.11 (d, *J* = 8.4 Hz, 2H, Ar-H in R), 6.73 (d, *J* = 8.4 Hz, 2H, Ar-H in R), 6.54 (d, *J* = 8.8 Hz, 1H, Ar-H), 6.38 (s, 1H, Ar-H), 6.04 (s, 1H, N-CH-O), 3.42 (q, *J* = 6.8 Hz, 4H, -$N(CH_2CH_3)_2$), 1.13 (t, *J* = 6.8 Hz, 6H, -$N(CH_2CH_3)_2$); LC/MS (ESI) m/z 364 $[M+H]^+$.

*7,9-Di-tert-butyl-2-(4-hydroxyphenyl)-3H-chromeno[2,3-d]pyrimidin-4(10aH)-one (**18**).* Yellow solid; mp = 248.9 ˚C; ^{1}H NMR (400 MHz, DMSO-d_6) δ 9.46 (s, 1H, OH), 8.56 (s, 1H, NH), 7.98 (s, 1H, Ar-H), 7.58 (d, *J* = 2.4 Hz, 1H, Ar-H), 7.44 (d, *J* = 2.4 Hz, 1H, Ar-H), 7.15 (d, *J* = 8.6 Hz, 2H, Ar-H in R), 6.75 (d, *J* = 8.6 Hz, 2H, Ar-H in R), 6.12 (s, 1H, N-CH-O), 1.40 (s, 9H, ^{t}Bu), 1.29 (s, 9H, ^{t}Bu); ^{13}C NMR (100 MHz, DMSO-d_6) δ 159.3, 157.6, 154.5, 150.3, 146.1, 135.8, 134.5, 133.4, 127.9, 127.7, 125.3, 119.4, 115.6, 114.2, 71.3, 35.0, 34.7, 31.5, 30.0; LC/MS (ESI) m/z 405 $[M+H]^+$.

*7-Isopropyl-2-phenyl-3,10a-dihydro-4H-chromeno[2,3-d]pyrimidin-4-one (**19**).* Yellow solid; ^{1}H NMR (400 MHz, DMSO-d_6) δ 8.99 (s, 1H, NH), 8.00 (s, 1H, Ar-H), 7.57 (d, *J* = 2.0 Hz, 1H, Ar-H), 7.42–7.32 (m, 6H, Ar-H), 7.13 (d, *J* = 8.4 Hz, 2H, Ar-H), 6.23 (s, 1H, N-CH-O), 2.94–2.87 (m, 1H, -*CH*$(CH_3)_2$), 1.21 (d, *J* = 6.8 Hz, 6H, -CH(CH_3)$_2$); LC/MS (ESI) m/z 319 $[M+H]^+$.

*7-Isopropyl-2-phenyl-3,5-dihydro-4H-chromeno[2,3-d]pyrimidin-4-one (**20**).* Pale yellow solid; ^{1}H NMR (400 MHz, DMSO-d_6) δ 8.13 (d, *J* = 7.6 Hz, 2H, Ar-H), 7.60–7.52 (m, 3H, Ar-H), 7.17–7.12 (m, 2H, Ar-H), 7.06 (d, *J* = 8.4 Hz, 2H, Ar-H), 3.73 (s, 2H, -CCH_2C-), 2.90–2.84 (m, 1H, -*CH*$(CH_3)_2$), 1.21 (d, *J* = 7.2 Hz, 6H, -CH(CH_3)$_2$); LC/MS (ESI) m/z 319 $[M+H]^+$.

*2-Benzyl-7-isopropyl-3,10a-dihydro-4H-chromeno[2,3-d]pyrimidin-4-one (**21**).* Pale yellow solid; ^{1}H NMR (400 MHz, CD_3OD) δ 7.58 (s, 1H, Ar-H), 7.38 (d, *J* = 8.4 Hz, 1H, Ar-H), 7.27 (s, 1H, Ar-H) 7.14–7.11 (m, 5H, Ar-H and NH), 7.07 (d, *J* = 8.4 Hz, 1H, Ar-H), 5.56 (t, *J* = 4.0 Hz, 1H, N-CH-O), 3.07–3.02 (m, 2H), 2.91–2.87 (m, 1H, -*CH*$(CH_3)_2$), 1.15 (d, *J* = 6.8 Hz, 6H, -CH(CH_3)$_2$); LC/MS (ESI) m/z 333 $[M+H]^+$.

*2-Cyclohexyl-7-isopropyl-3,10a-dihydro-4H-chromeno[2,3-d]pyrimidin-4-one (**22**).* Pale yellow solid; mp = 253.2 ˚C; ^{1}H NMR (400 MHz, DMSO-d_6) δ 8.51 (s, 1H, NH), 7.85 (s, 1H, Ar-H), 7.50 (d, *J* = 2.4 Hz, 1H, Ar-H), 7.38 (dd, *J* = 8.4 and 2.0 Hz, 1H, Ar-H), 7.12 (d, *J* = 8.4 Hz, 1H, Ar-H), 5.03 (s, 1H, N-CH-O), 2.92–2.85 (m, 1H, -*CH*$(CH_3)_2$), 2.56–2.45 (m, 1H, cyclohexyl in R) 1.72–1.55 (m, 6H, cyclohexyl in R), 1.26–0.86 (m, 4H, cyclohexyl in R), 1.20 (d, *J* = 6.8 Hz, 6H, -CH(CH_3)$_2$); ^{13}C NMR (100 MHz, DMSO-d_6) δ 160.1, 154.8, 152.2, 144.5, 132.8, 131.4, 127.4, 119.3, 115.8, 115.5, 72.9, 45.6, 33.1, 27.7, 26.5, 26.2, 26.0, 25.9, 24.2; LC/MS (ESI) m/z 325 $[M+H]^+$.

*2-Cyclopropyl-7-isopropyl-3,10a-dihydro-4H-chromeno[2,3-d]pyrimidin-4-one (**23**).* Pale yellow

solid; mp = 224.8 ˚C; ^{1}H NMR (400 MHz, DMSO-d_6) δ 8.70 (s, 1H, NH), 7.88 (s, 1H, Ar-H), 7.52 (d, *J* = 2.0 Hz, 1H, Ar-H), 7.39 (dd, *J* = 8.4 and 2.0 Hz, 1H, Ar-H), 7.11 (d, *J* = 8.4 Hz, 1H, Ar-H), 4.82 (d, *J* = 6.4 Hz, 1H, N-CH-O), 2.93–2.86 (m, 1H, -*CH*$(CH_3)_2$), 1.20 (d, *J* = 6.8 Hz, 6H, -CH(*CH_3*)$_2$), 1.16–1.10 (m, 1H, cyclopropyl in R), 0.45–0.33 (m, 4H, cyclopropyl in R); ^{13}C NMR (100 MHz, DMSO-d_6) δ 159.6, 154.8, 152.2, 144.6, 133.1, 131.5, 127.5, 119.2, 115.8, 115.2, 71.2, 33.1, 26.7, 24.2, 19.6, 1.9, 1.6; LC/MS (ESI) m/z 283 $[M+H]^+$.

*2,7-Diisopropyl-3,10a-dihydro-4H-chromeno[2,3-d]pyrimidin-4-one (**24**).* Pale yellow solid; ^{1}H NMR (400 MHz, CD_3OD) δ 7.95 (s, 1H, Ar-H), 7.44–7.42 (m, 2H, Ar-H), 7.12 (d, *J* = 9.2 Hz, 1H, Ar-H), 5.16 (dd, *J* = 3.4 and 1.0 Hz, 1H, N-CH-O), 2.98–2.91 (m, 1H, -*CH*$(CH_3)_2$), 2.04–1.96 (m, 1H, -*CH*$(CH_3)_2$ in R), 1.27 (d, *J* = 6.8 Hz, 6H, -CH(*CH_3*)$_2$), 1.00 (d, *J* = 6.8 Hz, 3H, -CH(*CH_3*)$_2$ in R), 0.93 (d, *J* = 6.8 Hz, 3H, -CH(*CH_3*)$_2$ in R); LC/MS (ESI) m/z 285 $[M+H]^+$.

*7-Isopropyl-2-(thiophen-2-yl)-3,10a-dihydro-4H-chromeno[2,3-d]pyrimidin-4-one (**25**).* Pale yellow solid; ^{1}H NMR (400 MHz, DMSO-d_6) δ 9.21 (s, 1H, NH), 8.03 (s, 1H, Ar-H), 7.58 (d, *J* = 2.0 Hz, 1H, Ar-H), 7.48–7.43 (m, 2H, Ar-H), 7.20–7.15 (m, 2H, Ar-H), 7.02–7.00 (m, 1H, Ar-H), 6.52 (s, 1H, N-CH-O), 2.95–2.88 (m, 1H, -*CH*$(CH_3)_2$), 1.21 (d, *J* = 6.8 Hz, 6H, -CH(*CH_3*)$_2$); LC/MS (ESI) m/z 325 $[M+H]^+$.

*2-(3-Hydroxyphenyl)-7-isopropyl-3,10a-dihydro-4H-chromeno[2,3-d]pyrimidin-4-one (**26**).* Yellow solid; ^{1}H NMR (400 MHz, DMSO-d_6) δ 9.43 (s, 1H, OH), 8.96 (s, 1H, NH), 8.00 (s, 1H, Ar-H), 7.57 (d, *J* = 2.0 Hz, 1H, Ar-H), 7.41 (dd, *J* = 8.4 and 2.4 Hz, 1H, Ar-H), 7.18–7.12 (m, 2H, Ar-H), 6.78–6.68 (m, 3H, Ar-H), 6.11 (s, 1H, N-CH-O), 2.94–2.87 (m, 1H, -*CH*$(CH_3)_2$), 1.21 (d, *J* = 7.2 Hz, 6H, -CH(*CH_3*)$_2$); LC/MS (ESI) m/z 335 $[M+H]^+$.

*2-(2-Hydroxyphenyl)-7-isopropyl-3,10a-dihydro-4H-chromeno[2,3-d]pyrimidin-4-one (**27**).* Pale yellow solid; ^{1}H NMR (400 MHz, DMSO-d_6) δ 9.66 (s, 1H, OH), 8.64 (s, 1H, NH), 7.94 (s, 1H, Ar-H), 7.55 (d, *J* = 2.4 Hz, 1H, Ar-H), 7.38 (dd, *J* = 8.4 and 2.0 Hz, 1H, Ar-H), 7.15–7.09 (m, 3H, Ar-H), 6.81–6.77 (m, 2H, Ar-H), 6.32 (s, 1H, N-CH-O), 2.93–2.87 (m, 1H, -*CH*$(CH_3)_2$), 1.21 (d, *J* = 7.2 Hz, 6H, -CH(*CH_3*)$_2$); LC/MS (ESI) m/z 335 $[M+H]^+$.

*2-(4-Fluorophenyl)-7-isopropyl-3,10a-dihydro-4H-chromeno[2,3-d]pyrimidin-4-one (**28**).* Yellow

solid; ^{1}H NMR (400 MHz, DMSO-d_6) δ 8.99 (s, 1H, NH), 8.00 (s, 1H, Ar-H), 7.57 (d, J = 2.0 Hz, 1H, Ar-H), 7.43–7.39 (m, 3H, Ar-H), 7.20 (t, J = 8.8 Hz, 2H, Ar-H), 7.13 (d, J = 8.4 Hz, 1H, Ar-H), 6.25 (s, 1H, N-CH-O), 2.94–2.87 (m, 1H, -*CH*(CH_3)$_2$), 1.21 (d, J = 6.8 Hz, 6H, -CH(*CH_3*)$_2$); LC/MS (ESI) m/z 337 $[M+H]^+$.

*2-(3-Fluorophenyl)-7-isopropyl-3,10a-dihydro-4H-chromeno[2,3-d]pyrimidin-4-one (**29**).* Pale yellow solid; ^{1}H NMR (400 MHz, DMSO-d_6) δ 9.02 (s, 1H, NH), 8.01 (s, 1H, Ar-H), 7.57 (s, 1H, Ar-H), 7.43–7.41 (m, 2H, Ar-H), 7.23–7.13 (m, 4H, Ar-H), 6.26 (s, 1H, N-CH-O), 2.92–2.87 (m, 1H, -*CH*(CH_3)$_2$), 1.21 (d, J = 6.8 Hz, 6H, -CH(*CH_3*)$_2$); LC/MS (ESI) m/z 337 $[M+H]^+$.

*7-Isopropyl-2-(3-methoxyphenyl)-3,10a-dihydro-4H-chromeno[2,3-d]pyrimidin-4-one (**30**).* Yellow solid; ^{1}H NMR (400 MHz, CD_3OD) δ 8.08 (s, 1H, NH), 7.47 (s, 1H, Ar-H), 7.45 (d, J = 8.8 Hz, 1H, Ar-H), 7.32 (t, J = 7.8 Hz, 1H, Ar-H), 7.15 (d, J = 8.0 Hz, 1H, Ar-H), 6.99–6.95 (m, 2H, Ar-H), 6.91 (dd, J = 8.0 and 2.4 Hz, 1H, Ar-H), 6.24 (s, 1H, N-CH-O), 3.80 (s, 3H, -OCH_3), 3.00–2.93 (m, 1H, -*CH*(CH_3)$_2$), 1.28 (d, J = 6.4 Hz, 6H, -CH(*CH_3*)$_2$); LC/MS (ESI) m/z 349 $[M+H]^+$.

*7-Isopropyl-2-(p-tolyl)-3,10a-dihydro-4H-chromeno[2,3-d]pyrimidin-4-one (**31**).* Yellow solid; ^{1}H NMR (400 MHz, DMSO-d_6) δ 8.95 (s, 1H, NH), 7.98 (s, 1H, Ar-H), 7.56 (d, J = 2.4 Hz, 1H), 7.40 (dd, J = 8.4 and 2.0 Hz, 1H, Ar-H), 7.23 (d, J = 8.4 Hz, 2H, Ar-H in R), 7.18 (d, J = 8.4 Hz, 2H, Ar-H in R), 7.12 (d, J = 8.4 Hz, 1H, Ar-H), 6.18 (s, 1H, N-CH-O), 2.94–2.87 (m, 1H, -*CH*(CH_3)$_2$), 2.29 (s, 3H, Ph-CH_3), 1.21 (d, J = 7.2 Hz, 6H, -CH(*CH_3*)$_2$); LC/MS (ESI) m/z 333 $[M+H]^+$.

*2-(4-Dimethylaminophenyl)-7-isopropyl-3,10a-dihydro-4H-chromeno[2,3-d]pyrimidin-4-one (**32**).* Yellow solid; ^{1}H NMR (400 MHz, DMSO-d_6) δ 8.87 (s, 1H, NH), 7.96 (s, 1H, Ar-H), 7.55 (d, J = 2.4 Hz, 1H), 7.40 (dd, J = 8.8 and 2.4 Hz, 1H, Ar-H), 7.14–7.11 (m, 3H, Ar-H), 6.70 (J = 8.8 Hz, 2H, Ar-H in R), 6.10 (s, 1H, N-CH-O), 2.92–2.87 (m, 1H, -*CH*(CH_3)$_2$), 2.87 (s, 6H, -N(CH_3)$_2$), 1.21 (d, J = 7.2 Hz, 6H, -CH(*CH_3*)$_2$); LC/MS (ESI) m/z 362 $[M+H]^+$.

*2-(3-Fluoro-4-hydroxyphenyl)-7-isopropyl-3,10a-dihydro-4H-chromeno[2,3-d]pyrimidin-4-one (**33**).* Yellow solid; ^{1}H NMR (400 MHz, DMSO-d_6) δ 8.92 (s, 1H, NH), 7.98 (s, 1H, Ar-H), 7.56 (d, J = 2.4 Hz, 1H, Ar-H), 7.41 (dd, J = 8.8 and 2.4 Hz, 1H, Ar-H), 7.14–7.10 (m, 2H, Ar-H), 6.99–6.91 (m, 2H, Ar-H), 6.14 (s, 1H, N-CH-O), 2.94–2.87 (m, 1H, -*CH*(CH_3)$_2$), 1.21 (d, J = 7.2 Hz, 6H, -

CH(CH_3)$_2$); ^{13}C NMR (100 MHz, DMSO-d_6) δ 159.3, 152.2, 145.1, 144.9, 144.7, 134.2, 133.8, 131.6, 127.6, 122.8, 119.3, 118.0, 115.9, 114.9, 114.7, 114.5, 70.5, 33.1, 24.2; LC/MS (ESI) m/z 353 $[M+H]^+$.

2-(2-Fluoro-4-hydroxyphenyl)-7-isopropyl-3,10a-dihydro-4H-chromeno[2,3-d]pyrimidin-4-one ***(34)****.* Yellow solid; ^{1}H NMR (400 MHz, DMSO-d_6) δ 9.96 (s, 1H, OH), 8.86 (s, 1H, NH), 7.99 (s, 1H, Ar-H), 7.56 (d, J = 2.4 Hz, 1H, Ar-H), 7.41 (dd, J = 8.8 and 2.4 Hz, 1H, Ar-H), 7.17–7.11 (m, 2H, Ar-H), 6.61–6.52 (m, 2H, Ar-H), 6.28 (s, 1H, N-CH-O), 2.94–2.87 (m, 1H, -*CH*(CH_3)$_2$), 1.21 (d, J = 7.2 Hz, 6H, -CH(CH_3)$_2$); LC/MS (ESI) m/z 353 $[M+H]^+$.

2-(4-Hydroxy-3-methoxyphenyl)-7-isopropyl-3,10a-dihydro-4H-chromeno[2,3-d]pyrimidin-4-one ***(35)****.* Pale yellow solid; ^{1}H NMR (400 MHz, DMSO-d_6) δ 9.01 (s, 1H, OH), 8.89 (s, 1H, NH), 7.97 (s, 1H, Ar-H), 7.55 (s, 1H, Ar-H), 7.40 (d, J = 8.8 Hz, 1H, Ar-H), 7.12 (d, J = 8.4 Hz, 1H, Ar-H), 6.91 (s, 1H, Ar-H), 6.77–6.72 (m, 2H, Ar-H), 6.13 (s, 1H, N-CH-O), 3.75 (d, J = 1.6 Hz, 3H, Ph-OCH_3)2.93–2.87 (m, 1H, -*CH*(CH_3)$_2$), 1.21(d, J = 7.2 Hz, 6H, -CH(CH_3)$_2$); ^{13}C NMR (100 MHz, DMSO-d_6) δ 159.3, 154.6, 152.2, 147.9, 146.8, 144.6, 133.8, 133.5, 131.6, 127.6, 119.3, 119.0, 115.9, 115.7, 115.0, 111.1, 71.2, 56.1, 33.1, 24.2; LC/MS (ESI) m/z 365 $[M+H]^+$.

2-(Benzo[d][1,3]dioxol-5-yl)-7-isopropyl-3,10a-dihydro-4H-chromeno[2,3-d]pyrimidin-4-one ***(36)****.* Yellow solid; ^{1}H NMR (400 MHz, DMSO-d_6) δ 8.91 (s, 1H, NH), 7.98 (s, 1H, Ar-H), 7.56 (s, 1H, Ar-H), 7.41 (d, J = 8.4 Hz, 1H, Ar-H), 7.13 (dd, J = 8.4 and 1.6 Hz, 1H, Ar-H), 6.90–6.82 (m, 3H, Ar-H), 6.15 (s, 1H, N-CH-O), 6.01 (d, J = 1.6 Hz, 2H, -OCH_2O-), 2.94–2.87 (m, 1H, -*CH*(CH_3)$_2$), 1.21 (d, J = 6.8 Hz, 6H, -CH(CH_3)$_2$); LC/MS (ESI) m/z 363 $[M+H]^+$.

2-(2,3-Dimethoxyphenyl)-7-isopropyl-3,10a-dihydro-4H-chromeno[2,3-d]pyrimidin-4-one ***(37)****.* Pale yellow solid; ^{1}H NMR (400 MHz, DMSO-d_6) δ 8.80 (s, 1H, NH), 7.98 (s, 1H, Ar-H), 7.56 (d, J = 2.0 Hz, 1H, Ar-H), 7.39 (dd, J = 8.4 and 2.4 Hz, 1H, Ar-H), 7.11–7.01 (m, 3H, Ar-H), 6.82 (dd, J = 7.6 and 2.0 Hz, 1H, Ar-H), 6.37 (s, 1H, N-CH-O), 3.81 (s, 3H, Ph-OCH_3), 3.72 (s, 3H, Ph-OCH_3), 2.94–2.87 (m, 1H, -*CH*(CH_3)$_2$), 1.21 (d, J = 7.2 Hz, 6H, -CH(CH_3)$_2$); LC/MS (ESI) m/z 379 $[M+H]^+$.

2-(2,3-Dimethylphenyl)-7-isopropyl-3,10a-dihydro-4H-chromeno[2,3-d]pyrimidin-4-one ***(38)****.* Pale yellow solid; mp = 231.6 ˚C; ^{1}H NMR (400 MHz, DMSO-d_6) δ 8.85 (s, 1H, NH), 7.99 (s, 1H, Ar-H), 7.55 (d, J = 2.4 Hz, 1H, Ar-H), 7.39 (dd, J = 8.8 and 2.4 Hz, 1H, Ar-H), 7.14–7.03 (m, 4H, Ar-H),

6.49 (s, 1H, N-CH-O), 2.93–2.86 (m, 1H, -*CH*(CH_3)$_2$), 2.29 (s, 3H, Ph-CH_3), 2.27 (s, 3H, Ph-CH_3), 1.21 (d, J = 6.8 Hz, 6H, -CH(*CH_3*)$_2$); ^{13}C NMR (100 MHz, DMSO-d_6) δ 159.4, 154.2, 151.8, 144.2, 140.0, 136.8, 133.6, 133.3, 133.0, 127.2, 127.0, 123.3, 118.8, 114.5, 68.8, 32.7, 32.6, 23.9, 23.6, 20.3, 20.1, 14.3, 14.1; LC/MS (ESI) m/z 347 $[M+H]^+$.

4.2. Cell lines and cell cultures

Human melanoma cell lines (A375, SK-MEL28, WM266-4 and SK-MEL2) and other cell lines (A549, MDA-MB231, DU145 and T47D) were purchased from American Type Culture Collection (ATCC, USA), and the other human melanoma cell lines (WM1366, WM3670) were obtained from Coriell (Coriell Institute for Medical Research, USA). Human cell lines (A375, SK-MEL28, WM266-4, A549, MDA-MB231, DU145 and T47D) were maintained in DMEM high glucose (Gibco, USA) supplemented with 10 % fetal bovine serum (FBS, Gibco, USA) and 1 % penicillin, streptomycin and 1 % sodium pyruvate (Gibco, USA). SK-MEL2 was cultured in ATCC-formulated Eagle's Minimum Essential Medium (EMEM, ATCC, USA) containing 10 % FBS. The other melanoma cell lines (WM1366, WM3670) were cultured in 4:1 mixture of MCDB153 (WelGENE Inc., Korea) and Leibovitz L-15 (Gibco, USA), supplemented with 2 % FBS, 5 μg/mL of insulin (Gibco, USA) and 1.68 mM of $CaCl_2$ (Withlab Co., Ltd, Korea) in 37 ˚C, 5 % CO_2 atmosphere at constant humidity. WM1366 and WM3670 cells were cultured on bio-coated flask (BD Biosciences, USA). All cell lines were mycoplasma free when periodically tested with the MycoAlert™ Mycoplasma Detection Kit (Lonza, USA).

4.3. Senescence screening assay

The compounds were added to the assay plate (Evotec™ 384-well microplate, Germany) with 10 μL DMEM (Gibco, USA) supplemented with 1.0 mmol/L sodium pyruvate, 1 % streptomycin/penicillin and 10 % heat-inactivated FBS using Hummingbird. A375 cells were cultivated in DMEM (Gibco, USA) medium supplemented with 1.0 mmol/L sodium pyruvate, 1 % streptomycin/penicillin and 10 % heat-inactivated FBS at 37 ˚C and 5 % CO_2. After compound

addition, cells (5×10^4 cells/mL) were diluted in DMEM supplemented with 1.0 mmol/L sodium pyruvate, 1 % streptomycin/penicillin and 10 % heat-inactivated FBS, seeded in 40 μL per well using WELLMATE (Thermo Scientific Matrix WellMate, USA) and incubated at 37 ˚C for 72 hrs. Doxorubicin hydrochloride as the reference compound (positive control) at 37 nM as the EC_{100} and 0.5 % DMSO (negative control) were used in all the plates for data normalization. After 3 days of incubation, the assay plates were stained with Hoechst33342 (Invitrogen, USA), LysoTracker® Red DND-99 (Invitrogen, USA) and CellMask™ Deep Red Plasma membrane Stain (Invitrogen, USA) for 1 hr. Microplates were read in an Opera® High Content Screening System (PerkinElmer Inc., USA), enabling the determination of the senescence effect ratio by image analysis. An algorithm for image analysis was developed to determine senescence effects and count cell number. With this technique, the senescence was determined by 130 descriptions such as cell size, nucleus size, texture of cells etc. The average senescent ratios from the positive and negative controls were normalized to 0 % and 100 % senescence effect, and the senescent ratio read from each compound activity was proportionally distributed within this range. Z-factor was used for protocol validation and active compound selection acceptance. Z-factor, calculated as $1-[3(\sigma_p+\sigma_n)/(\mu_p-\mu_n)]$, where μ_p, σ_p, μ_n and σ_n are the means (μ) and standard deviations (σ) of both the positive (p) and negative (n) controls, and other parameters, including DRC control for verification of the reference drug EC_{50} (accepted if within the range of 3× higher or lower than a defined value from the literature), coefficient of variation not higher than 10 % in the controls and edge effect evaluation, were used for screening validation and hits selection.

4.4. Double strand DNA and single strand DNA assay

For checking double DNA damage of cells, cells were seeded in 384-well plates (2×10^3 cells/well), and exposed to dose response concentration (DRC) of a compound from 0 to 20 μM for 3 days. And then cells were fixed in 4 % paraformaldehyde (WAKO, Japan) for 20 min at room temperature and washed twice in PBS (WelGENE Inc., Korea) and permeabilized in 0.5 % Triton X-100 (Sigma, USA) in PBS for 15 min. Cells were washed twice in PBS and blocked for 1 hr in 3 % BSA (Sigma, USA)

in PBS containing Tween-20 (PBST, Sigma, USA), after which they were incubated in anti-53BP1 (Millipore, USA) and anti-γH2AX (Millipore, USA) in 1 % BSA-PBST buffer for overnight at 4 ˚C. After 24 hrs, cells were washed three times in PBST and incubated in Alexa Fluor® 488 goat anti-mouse and Alexa Fluor® 532 goat anti-rabbit secondary antibody (Invitrogen, USA) in 1 % BSA-PBST for 1 hr at room temperature to label 53BP1 and γ-H2AX. Cells were washed three times for 10 min, stained with Hoechst (Invitrogen, USA) for 20 min, and then washed three times for 10 min. The images were photographed at 20× water magnifications using Opera®. To measure single-stranded DNA, we purchased Quant-iT™ OliGreen® ssDNA Assay Kit (Invitrogen, USA) and followed a procedure in manual as described.

4.5. Senescence-associated β-galactosidase (SA-β-gal) assay

A375 cells in 96-well plates (4×10^2 cells/well) were incubated with 0.5 % DMSO and **3** for 72 hrs. After 3 days, the adherent cells were fixed for 20 min at room temperature in 0.2 % glutaraldehyde (Sigma, USA) and stained for 3 days at 37 ˚C freshly prepared X-Gal staining solutions (pH 6.0) containing 1 mM $MgCl_2$, 0.1 mg/mL X-Gal (Invitrogen, USA), 5 mM potassium ferricyanide (Sigma, USA), and 5 mM potassium ferrocyanide (Sigma, USA). The images were photographed at several magnifications using a microscopy.

4.6. Colony formation assay

Cells in 96-well plates (20 cells/well) were seeded and incubated with a compound for 3 days. And then the fresh media was replaced for 4 days. Seven days after seeding, cells were fixed in 4 % paraformaldehyde (WAKO, Japan) at room temperature for 20 min, washed twice with PBS. Next, cells were stained with 0.1 % crystal violet (Sigma, USA) in PBS for 20 min at room temperature. Stained surviving cells were photographed.

4.7. Flow cytometry analysis of cell cycle

Human melanoma A375 cells were incubated with a compound (20 μM) for 72 hrs, and harvested up to 1 × 106 cells/100 μL into FACS tubes. They were washed 2 times by adding 2 mL of PBS (or HBSS), centrifuged for 5 min at 300 × g, and then resuspended in 1 mL of flow cytometry staining buffer (R&D Systems, USA). After adding 1 μL of propidium iodide staining solution (1 mg/mL, Sigma, USA), cells were analyzed by BD FACSAria™ III (BD Biosciences, USA).

4.8. Microsomal metabolic stability

Human liver microsomes (mixed gender, pool of 200) were purchased from XenoTech (Lenexa, USA). Mouse male microsomes and nicotinamide adenine dinucleotide phosphate (NADPH) regenerating system were purchased from BD Gentest (Woburn, USA). A Quattro Premier™ triple quadrupole mass spectrometer (Waters, USA) with electrospray ionization (ESI) was applied for sample analysis. Instruments were controlled by Masslynx software (Version 4.0, Waters, USA). An analytical column was applied after the trapping cartridges (Agilent, Zorbax Eclipse plus RRHD C18, 50 mm × 2.1 mm, 1.8 μm, USA). Compounds (2 μM as final concentration) are incubated with both human and mouse liver microsomes in potassium phosphate buffer at 37 ˚C. The microsomal protein concentration in the assay was 0.5 mg/mL and the final percent of DMSO was 0.2 %. Reaction was started by the addition of NADPH and terminated either immediately or at 10, 20, 30 and 60 min for a precise estimate of clearance. The corresponding loss of parent compound was determined by LC/MS. The mobile phases were (A) water with 0.1 % of formic acid and (B) acetonitrile with 0.1 % of formic acid at a flow rate of 0.4 mL/min. The LC conditions were 10 % B at 0 min, a linear gradient from 10 to 90 % B over 0.25 min, held at 90 % B for 0.7 min, and back to 10 % B over 0.2 min, then held at 10 % B for the remaining 0.6 min. The percentage of remaining compound was calculated by comparing with the initial quantity at time 0 min. Half-life was then calculated, based on first-order reaction kinetics.

4.9. Glucuronidation assay using S9 fraction

Human liver S9 (mixed gender, pool of 200) were purchased from XenoTech (Lenexa, USA). Mouse male S9 and uridine glucuronosyl transferase (UGT) mix solution were purchased from BD Gentest (Woburn, USA). Compounds (2 μM as final concentration) were incubated with both human and mouse liver S9 fraction in Tris buffer at 37 ˚C. The S9 protein concentration in the assay was 1.0 mg/mL and the final percent DMSO was 0.2 %. Reaction was started by the addition of 25 mM uridine diphosphate glucuronic acid (UDPGA) to result in a final UDPGA concentration of 2 mM and terminated either immediately or at 10, 20, 30 and 60 min for a precise estimate of clearance. Half-life was calculated, based on first-order reaction kinetics.

4.10. In vivo pharmacokinetics study

Male balb/c mice (8 weeks old) were used for pharmacokinetic studies. Compound **38** were administered by intravenous bolus, oral (PO) or intraperitoneal (IP) injection. The compound were formulated in 5 % DMSO and 20 % hydroxypropyl-β-cyclodextrin (HP-β-CD) for the study. Blood samples were collected from the animals *via* retro-orbital venous plexus by at 0.033, 0.25, 0.5, 1, 2, 4, 6, 8 and 24 hrs post-dose for IV. For PO and IP, blood samples were taken at 0.083, 0.25, 0.5, 1, 2, 4, 6, 8 and 24 hrs post-dose. Blood samples were collected into tubes pretreated with EDTA and centrifuged at 3,200 g for 10 min at 4 ˚C. Following centrifugation, plasma was transferred into tubes and frozen prior to LC-MS/MS analysis. Analysis of plasma samples were conducted on Quattro Premier™ triple quadrupole mass spectrometer (Waters, USA) coupled with Acquity® ultra performance liquid chromatography (Waters, USA).

4.11. Pharmacophore modeling

A dataset of 36 compounds in Table 1 was used to build a pharmacophore model based on their activities inducing senescence-like phenotype (EC_{50}). All structures were built on Maestro, a module of Schrödinger [45]. Low energy 3D conformations of compounds were processed with the LigPrep program [46], and they were energy minimized with OPLS_2005 force field method. Next, the conformers were generated for each compound by using a torsional search method with ConfGen [47].

Total of 100 conformers per rotatable bonds were generated with the maximum number of conformers set as 1,000 per compound. The minimization and energy calculation were done by applying OPLS_2005 force field. The activity value for each compound was taken as a negative logarithm of EC_{50} value. The activities of synthetic derivatives have been classified as follows: 10 active analogues (-log EC_{50} > 1.0), 12 moderately active analogues (0.0 < -log EC_{50} < 1.0) and 14 inactive analogues (-log EC_{50} ≤ 0.0). Phase program was used to generate common pharmacophore hypothesis (CPH) [48]. Initially, pharmacophores generated for all conformations of synthetic derivatives were examined, and then pharmacophore models having common features were identified as CPH. Hypotheses were generated by a systematic variation of minimum and maximum number of sites set to 6, and to match all 10 active analogues. The best CPH was selected to have high ranking scores overall across various scoring terms such as survival score.

ASSOCIATED CONTENT

The Supporting Information is available free of charge on the ACS Publications website at DOI:----------.

Characterization data of **3**–**38** including ^{1}H, and / or ^{13}C (PDF)

Molecular formula strings (CSV)

AUTHOR INFORMATION

Corresponding authors

Tel.: +82-31-698-3832; fax: +82-31-698-3842; e-mail: rtsong@hanaph.co.kr

Tel.: +82-2-527-5036; fax: +82-2-527-5020; e-mail: nanmolra1973@naver.com

Notes

The authors declare no competing financial interest.

ACKNOWLEDGEMENTS

This work was supported by the National Research foundation of Korea (NRF) grant funded by the Korea government (MSIP, No. 2007-00559, No. 2010-0024957 and MSIT (NRF-2017M3A9G6068257) , Gyeonggi-do and KISTI.

ABBREVIATIONS USED

TIS, therapy-induced senescence; HTS, high-throughput screening; HCS, high-contents screening; SAR, structure-activity relationship; FDA, U.S. Food and Drug Administration; SA-β-gal, senescence-associated beta-galactosidase; DMSO, dimethyl sulfoxide; DDR, DNA damage response; SSB, single-strand break; DSBs, double-stranded breaks; NMR, nuclear magnetic resonance; ESI, electrospray ionization; CPH, common pharmacophore hypotheses; LC/MS, liquid chromatography/mass spectrometry; TLC, thin-layer chromatography; DRC, dose-response curve.

References

[1] American Cancer Society: Cancer Facts and Figures 2019. Atlanta, GA: American Cancer Society 2019.

[2] R.L. Siegel, K.D. Miller, A. Jemal, Cancer statistics, 2019, CA Cancer J. Clin. 69 (2019) 7–34.

[3] http://www.cancer.org/cancer/skincancer-melanoma/detailedguide/melanoma-skin-cancer-survival-rates.

[4] N. Howlader, A.M. Noone, M. Krapcho, D. Miller, A. Brest, M. Yu, J. Ruhl, Z. Tatalovich, A. Mariotto, D.R. Lewis, H.S. Chen, E.J. Feuer, D.A. Cronin, SEER Cancer Statistics Review, 1975–2016, National Cancer Institute. Bethesda, MD, https://seer.cancer.gov/csr/1975_2016/, based on November 2018 SEER data submission, posted to the SEER web site, April 2019.

[5] A. Mullard, Dual fronts poised to transform melanoma therapy, Nat. Rev. Drug Discov. 10 (2011), 325–326.

[6] G. Bollag, J. Tsai, J. Zhang, C. Zhang, P. Ibrahim, K. Nolop, P. Hirth, Vemurafenib: the first drug approved for BRAF-mutant cancer, Nat. Rev. Drug Discov. 11 (2012), 873–886.

[7] E.J. Lipson, C.G. Drake, Ipilimumab: an anti-CTLA-4 antibody for metastatic melanoma, Clin. Cancer Res. 17 (2011), 6958–6962.

[8] J.S. Weber, K.C. Kähler, A. Hauschild, Management of immune-related adverse events and kinetics of response with ipilimumab, J. Clin. Oncol. 30 (2012) 2691–2697.

[9] M.K. Callahan, M.A. Postow, J.D. Wolchok, Immunomodulatory therapy for melanoma: ipilimumab and beyond, Clin. Dermatol. 31 (2013), 191–199.

[10] F. Su, W.D. Bradley, Q. Wang, H. Yang, L. Xu, B. Higgins, K. Kolinsky, K. Packman, M.J. Kim, K. Trunzer, R.J. Lee, K. Schostack, J. Carter, T. Albert, S. Germer, J. Rosinski, M. Martin, M.E. Simcox, B. Lestini, D. Heimbrook, G. Bollag, Resistance to selective BRAF inhibition can be mediated by modest upstream pathway activation, Cancer Res. 72 (2012), 969–978.

[11] M.D. Thakur, F. Salangsang, A.S. Landman, W.R. Sellers, N.K. Pryer, M.P. Levesque, R. Dummer, M. McMahon, D.D. Stuart, Modelling vemurafenib resistance in melanoma reveals a strategy to forestall drug resistance, Nature 494 (2013), 251–255.

[12] H. Berman, J. Westbrook, Z. Feng, G. Gilliland, T. Bhat, H. Weissig, I. Shindyalov, P. Bourne, The protein data bank, Nucleic Acids Res. 28 (2000), 235–242.

[13] C.A. Schmitt, Cellular senescence and cancer treatment, Biochim. Biophys. Acta 1775 (2007), 5–20.

[14] S. Lee, J.-S. Lee, Cellular senescence: A promising strategy for cancer therapy, BMB Rep. 52 (2019) 35–41.

[15] A. Vilgelm, A. Richmond, Combined therapies that induce senescence and stabilize p53 block melanoma growth and prompt antitumor immune responses, Oncoimmunology, 4 (2015), e1009299.

[16] L. Wang, R.L. de Oliveira, C. Wang, J.M.F. Neto, S. Mainardi, B. Evers, C. Lieftink, B. Morris, F. Jochems, L. Willemsen, R.L. Beijersbergen, R. Bernards, High-throughput functional genetic and compound screens identify targets for senescence induction in cancer, Cell Reports 21 (2017), 773–783.

[17] J.A. Ewald, J.A. Desotelle, G. Wilding, D.F. Jarrard, Therapy-induced senescence in cancer, J. Natl. Cancer Inst. 102 (2010), 1536–1546.

[18] A. Laine, H. Sihto, C. Come, M.T. Rosenfeldt, A. Zwolinska, M. Niemelä, A. Khanna, E.K. Chan, V.-M. Kähäri, P.-L. Kellokumpu-Lehtinen, O.J. Sansom, G.I. Evan, M.R. Junttila, K.M. Ryan, J.-C. Marine, H. Joenssu, J. Westermarck, Senescence sensitivity of breast cancer cells is defined by positive feedback loop

between CIP2A and E2F1, Cancer Discov. 3 (2013), 182–197.
[19] S. Haferkamp, A. Borst, C. Adam, T.M. Becker, S. Motschenbacher, S. Windhövel, A.L. Hufnagel, R. Houben, S. Meierjohann, Vemurafenib induces senescence features in melanoma cells, J. Investig. Dermatol. 133 (2013), 1601–1609.
[20] H. Luo, C. Yount, H. Lang, A. Yang, E.C. Riemer, K. Lyons, K.N. Vanek, G.A. Silvestri, B.A. Schulte, G.Y. Wang, Activation of p53 with Nutlin-3a radiosensitizes lung cancer cells via enhancing radiation-induced premature senescence, Lung Cancer 81 (2013), 167–173.
[21] S. Giuliano, M. Ohanna, R. Ballotti, C. Bertolotto, Advances in melanoma senescence and potential clinical application, Pigment Cell Melanoma Res. 24 (2011), 295–308.
[22] C.A. Schmitt, J.S. Fridman, M. Yang, S. Lee, E. Baranov, R.M. Hoffman, S.W. Lowe, A senescence program controlled by p53 and $p16^{INK4a}$ contributes to the outcome of cancer therapy, Cell 109 (2002), 335–346.
[23] M. Braig, C.A. Schmitt, Oncogene-induced senescence: putting the brakes on tumor development, Cancer Res. 66 (2006), 2881–2884.
[24] Z. Chen, L.C. Trotman, D. Shaffer, H.-K. Lin, Z.A. Dotan, M. Niki, J.A. Koutcher, H.I. Scher, T. Ludwig, W. Gerald, C. Cordon-Cardo, P.P. Pandolfi, Crucial role of p53-dependent cellular senescence in suppression of Pten-deficient tumorigenesis, Nature 436 (2005), 725–730.
[25] E.L. Denchi, C. Attwooll, D. Pasini, K. Helin, Deregulated E2F activity induces hyperplasia and senescence-like features in the mouse pituitary gland, *Mol. Cell. Biol.* 25 (2005), 2660–2672.
[26] C. Michaloglou, L.C. Vredeveld, M.S. Soengas, C. Denoyelle, T. Kuilman, C.M. Van Der Horst, D.M. Majoor, J.W. Shay, W.J. Mooi, D.S. Peeper, $BRAF^{E600}$-associated senescence-like cell cycle arrest of human naevi, Nature 436 (2005), 720–724.
[27] I.B. Roninson, Tumor cell senescence in cancer treatment, Cancer Res. 63 (2003), 2705–2715.
[28] R.H. te Poele, A.L. Okorokov, L. Jardine, J. Cummings, S.P. Joel, DNA damage is able to induce senescence in tumor cells *in vitro* and *in vivo*, Cancer Res. 62 (2002), 1876–1883.
[29] R.S. Roberson, S.J. Kussick, E. Vallieres, S.-Y.J. Chen, D.Y. Wu, Escape from therapy-induced accelerated cellular senescence in p53-null lung cancer cells and in human lung cancers, Cancer Res. 65 (2005), 2795–2803.
[30] B.C. Kim, H.J. Yoo, H.C. Lee, K.-A. Kang, S.H. Jung, H.-J. Lee, M. Lee, S. Park, Y.-H. Ji, Y.-S. Lee, Y.-G. Ko, J.-S. Lee, Evaluation of premature senescence and senescence biomarkers in carcinoma cells and xenograft mice exposed to single or fractionated irradiation, Oncol. Rep. 31 (2014), 2229–2235.
[31] J.A. Ewald, N. Peters, J.A. Desotelle, F.M. Hoffmann, D.F. Jarrard, A high-throughput method to identify novel senescence-inducing compounds, J. Biomol. Screen. 14 (2009), 853–858.
[32] B.G. Bitler, L.S. Fink, Z. Wei, J.R. Peterson, R. Zhang, A high-content screening assay for small-molecule modulators of oncogene-induced senescence, J. Biomol. Screen. 18 (2013), 1054–1061.
[33] M.A. Sliwinska, G. Mosieniak, K. Wolanin, A. Babik, K. Piwocka, A. Magalska, J. Szczepanowska, J. Fronk, E. Sikora, Induction of senescence with doxorubicin leads to increased genomic instability of HCT116 cells, Mech. Ageing Dev. 130 (2009), 24–32.
[34] M.-Y. Yang, P.-M. Lin, Y.-C. Liu, H.-H. Hsiao, W.-C. Yang, J.-F. Hsu, C.-M. Hsu, S.-F. Lin, Induction of cellular senescence by doxorubicin is associated with upregulated *miR*-375 and induction of autophagy in K562

cells, PloS One 7 (2012), e37205.

[35] A. Bielak-Zmijewska, M. Wnuk, D. Przybylska, W. Grabowska, A. Lewinska, O. Alster, Z. Korwek, A. Cmoch, A. Myszka, S. Pikula, G. Mosieniak, E.A. Sikora, A comparison of replicative senescence and doxorubicin-induced premature senescence of vascular smooth muscle cells isolated from human aorta, Biogerontology 15 (2014), 47–64.

[36] T. Kuilman, C. Michaloglou, W.J. Mooi, D.S. Peeper, The essence of senescence, Genes Dev. 24 (2010), 2463–2479.

[37] S.E. Polo, S.P. Jackson, Dynamics of DNA damage response proteins at DNA breaks: a focus on protein modifications, Genes Dev. 25 (2011), 409–433.

[38] L.-J. Mah, A. El-Osta, T. Karagiannis, γH2AX: a sensitive molecular marker of DNA damage and repair, Leukemia 24 (2010), 679–686.

[39] A. Fradet-Turcotte, M.D. Canny, C. Escribano-Díaz, A. Orthwein, C.C. Leung, H. Huang, M.-C. Landry, J. Kitevski-LeBlanc, S.M. Noordermeer, F. Sicheri, D. Durocher, 53BP1 is a reader of the DNA-damage-induced H2A Lys 15 ubiquitin mark, Nature 499 (2013), 50–54.

[40] S. Cruet-Hennequart, Á.M. Prendergast, G. Shaw, F.P. Barry, M.P. Carty, Doxorubicin induces the DNA damage response in cultured human mesenchymal stem cells. Int. J. Hematol. 96 (2012), 649−656.

[41] D.E. Joyner, J.D. Bastar, R.L. Randall, Doxorubicin induces cell senescence preferentially over apoptosis in the FU-SY-1 synovial sarcoma cell line. J. Orthop. Res. 24 (2006), 1163−1169.

[42] H. Tsao, L. Chin, L.A. Garraway, D.E. Fisher, Melanoma: from mutations to medicine. Genes Dev. 26 (2012), 1131−1155.

[43] C.N. O'Callaghan, Isomerisation of 2-aryl-4-oxo-2, 3-dihydrobenzopyrano [2,3-*d*] pyrimidines to 2-aryl-4-hydroxy-5*H*-benzopyrano [2,3-*d*] pyrimidines. J. Chem. Soc. Perkin 1 (1980), 1335−1337.

[44] A.V. Borisov, S.G. Dzhavakhishvili, I.O. Zhuravel, S.M. Kovalenko, V.M. Nikitchenko, Parallel liquid-phase synthesis of benzopyrano [2,3-*d*] pyrimidine libraries. J. Comb. Chem. 9 (2007), 5−8.

[45] Maestro, version 9.3, Schrödinger, LLC, New York, NY, 2012.

[46] LigPrep, version 2.6, Schrödinger, LLC, New York, NY, 2012.

[47] ConfGen, version 2.6, Schrödinger, LLC, New York, NY, 2012.

[48] Phase, version 3.4, Schrödinger, LLC, New York, NY, 2012.